Three-dimensional Image Processing Techniques to Perform Landmarking and Segmentation of Computed Tomographic Images

Rangaraj M. Rangayyan, Shantanu Banik, Graham S. Boag

Department of Electrical and Computer Engineering
University of Calgary
Alberta Children's Hospital
Calgary, Alberta, Canada.

Introduction

Identification and segmentation of the thoracic, abdominal, and pelvic organs are important steps in

- computer-aided diagnosis,
- treatment planning,
- landmarking, and
- content-based retrieval of biomedical images.

Computer-aided Diagnosis (CAD)

Manual segmentation and analysis of an organ or region of interest can provide accurate assessment, but are:

- tedious,
- time-consuming, and
- subject to intra- and inter-operator error.

Computer-aided Diagnosis (CAD)

Computer-aided analysis of medical images could facilitate quantitative and objective analysis.

Physicians could use the results of computer analysis as a "second opinion" to make the final decision.

Segmentation of Medical Images

For improved localization, segmentation, and analysis of various organs, the following approaches could be used:

- prior knowledge (knowledge-based),
- anatomical atlases (atlas-based),
- anatomical landmarks (landmark-based), and
- relative coordinate systems (landmark-based).

Landmarking of Medical Images

- Landmarks are used as references to represent the spatial relationship between different regions, organs, and structures in medical images.

- Landmarks are selected such that they:
  - are easy to detect,
  - have stable locations, and
  - have characteristics that do not vary to a large extent in the presence of abnormalities.

Tissue Characterization in Computed Tomographic (CT) Images

- As an X-ray beam traverses the body, it is attenuated according to Lambert-Beer law:

$$I_t = I_0 \exp(-\mu l)$$

I_t: transmitted intensity of the X ray,

I_0: incident intensity,

l : length of the path of the beam, and

μ: linear attenuation coefficient.

Hounsfield Units (HU)

- To represent μ in a more convenient manner and to make it effectively independent of the X-ray energy:

$$\text{CT number} = k\frac{\mu - \mu_w}{\mu_w}$$

μ_w: linear attenuation coefficient of water

k: scaling constant

- If $k = 1000$: **Hounsfield units (HU)**.

CT Values of Abdominal Tissues

	CT value (HU)	
Tissue	**Mean**	**SD**
Air	-1006	2
Fat	-90	18
Skin	+16	11
Spinal Canal	+23	15
Kidney	+32	10
Blood (Aorta)	+42	18
Muscle	+44	14
Spleen	+46	12
Necrosis	+45	15
Liver	+60	14
Viable Tumor	+91	25
Calcification	+345	155
Bone	+1005	103

Segmentation of CT Images: Motivation

- Most of the published procedures are only applicable to CT scans of adults.
- In pediatric cases, organs and tissues are not well developed, and possess different density or HU values than those for adults.
- This work is on segmentation and analysis of CT images of pediatric patients with tumors due to neuroblastoma in thoracic, abdominal, and pelvic regions.

Proposed Study

- Automatic segmentation of
  - the rib structure,
  - the vertebral column,
  - the spinal canal,
  - the diaphragm, and
  - the pelvic girdle.
- Use of these landmarks in the segmentation of abdominal tumors (neuroblastoma).

Image Processing: Segmentation

- Process of partitioning an image into regions representing the different objects in the image.

- Based on one of the two basic properties:
  - discontinuity and
  - similarity.

Histogram

- The histogram of a digital image $f(x, y)$ of size $M \times N$ with L gray levels is defined as:

$$P_f(l) = \sum_{x=0}^{M-1} \sum_{y=0}^{N-1} \delta[f(x,y) - l], \quad l = 0, 1, 2, \ldots, L-1$$

where the delta function $\delta(n)$ is defined as

$$\delta(n) \equiv \begin{cases} 1, & \text{for } n = 0 \\ 0, & \text{otherwise} \end{cases}$$

- The sum of all the entries in the histogram is equal to the total number of pixels (or voxels) in the image.

Histogram

If the image has large number of pixels (or voxels), the histogram will approximate the probability density function (PDF) of the gray levels in the image.

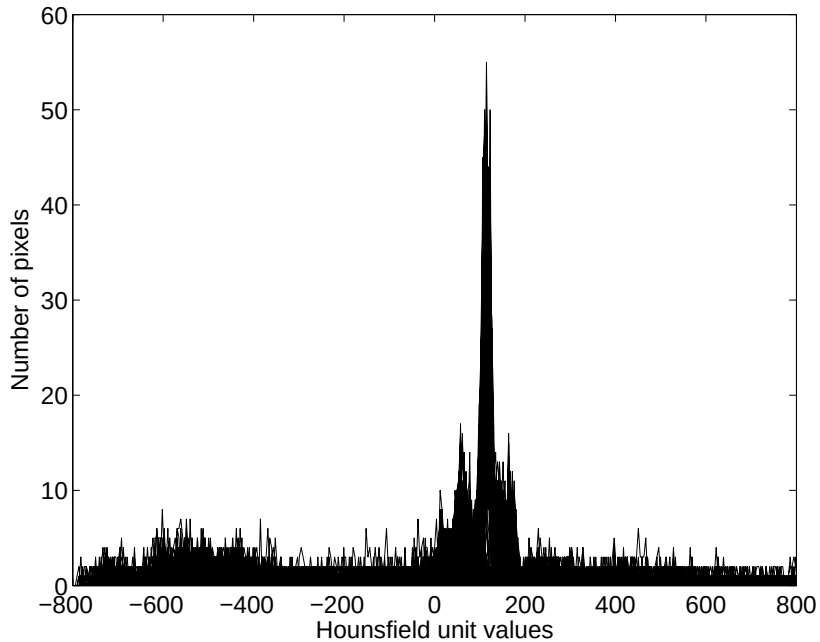

Thresholding

- Gray level thresholding segments an image based on the value at each point (x, y) or pixel relative to a specified threshold value, T.
- Thresholding can be local or global.
- In the simplest case, known as binarization, a single threshold is specified

$$g(x,y) = \begin{cases} 1, & \text{if } f(x,y) > T \\ 0, & \text{if } f(x,y) \leq T \end{cases}$$

where $T \in G$; G is the set of available values for gray levels.

Thresholding

- The use of multiple thresholds to perform segmentation is known as multi-thresholding.
- A set of thresholds, $T = \{T_0, T_1, T_2, \ldots, T_k\}$, is defined such that all elements in the image satisfying $f(x, y) = [T_{i-1}, T_i), i = 1, 2, \ldots, k$, constitute the i^{th} segmented region.
- In order to be effective good separation between the values of objects of interest and the background is required.

Thresholding

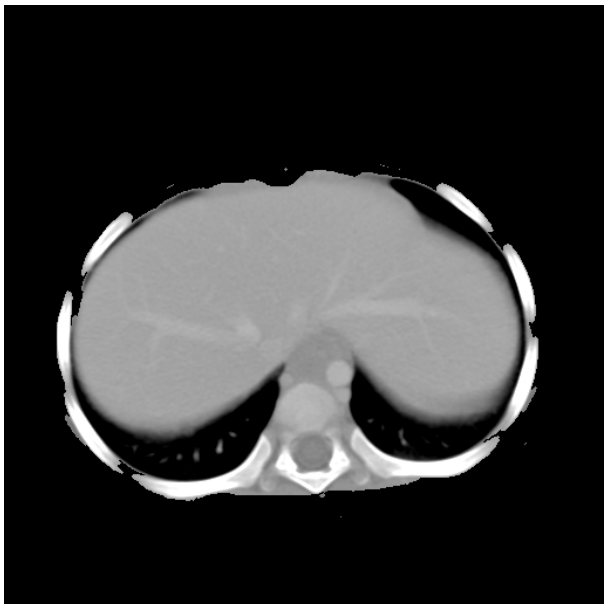

Original image

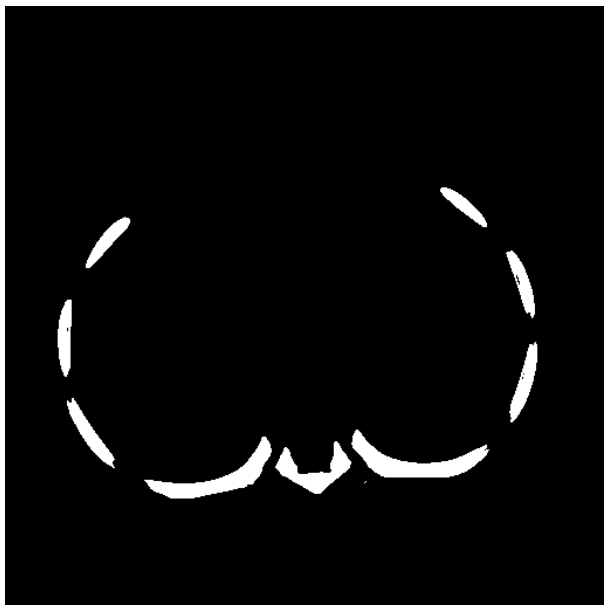

Thresholding at
T = 200 HU

Multi-thresholding at
T_0 = 0 HU, T_1 = 200 HU

Region-based Methods

If R represents the entire image region and segmentation results in n subregions, $R_1, R_2, \ldots, R_n$, the results should satisfy

1. $\bigcup_{i=1}^{n} R_i = 1\ R_i = R$,
2. R_i is a connected region, $i = 1, 2, \ldots, n$,
3. $R_i \cap R_j = \varnothing$ for all $i \neq j$,
4. $\mathcal{P}(R_i) = \text{TRUE}$ for all $i = 1, 2, \ldots, n$,
5. $\mathcal{P}(R_i \cup R_j) = \text{FALSE}$ for all $i \neq j$,

where $\mathcal{P}(R_i)$ is a logical predicate defined over the points or pixels in the set R_i, and $\varnothing$ is the null set.

Region Growing

- Region-based methods can be divided into two groups: region growing, and region splitting and merging.
- Region growing groups pixels or subregions into larger regions based on predefined criteria and connectivity.
- The result depends on:
  - selection of seed pixel or pixels,
  - specification of inclusion or similarity criteria, and
  - formulation of stopping rule.

Region Splitting and Merging

- Splitting is used to subdivide the entire region successively into smaller and smaller disjoint regions until the homogeneity criterion is satisfied by each region.
- Region splitting could result in adjacent regions with identical or similar properties.
- Merging allows neighboring homogeneous subregions to be combined into larger regions.

Edge-based Techniques

- An edge is the oriented boundary between two regions with relatively distinct gray-level properties.
- Most edge detection techniques require the computation of a local derivative or difference.
- The gradient of an image $f(x, y)$ at the location (x, y) is defined as the vector

$$\nabla \mathrm{f} = \begin{bmatrix} G_x \\ \\ G_y \end{bmatrix} = \begin{bmatrix} \dfrac{\partial f}{\partial x} \\ \\ \dfrac{\partial f}{\partial y} \end{bmatrix}$$

Gradient

- The magnitude of the gradient vector is given by

$$\nabla f = \left|\nabla \mathbf{f}\right| = \left[G_x^2 + G_y^2\right]^{1/2}$$

- The direction (angle) of the gradient vector is given by

$$\alpha(x, y) = \tan^{-1}\left(\frac{G_y}{G_x}\right)$$

where the angle is measured with respect to the x axis.

Edge Detection in Digital Images

- In digital images, the magnitude of the gradient is approximated by first difference operations:

$$G_x(x,y) = f(x,y) - f(x-1,y),$$

$$G_y(x,y) = f(x,y) - f(x,y-1).$$

Original image

Gradient magnitude, display range [5, 150] out of [0, 2371].

Edge Detection in Digital Images

- Among the difference-based edge detection operators, the Prewitt and Sobel operators are simple and popular.

$$\begin{bmatrix} -1 & -1 & -1 \\ 0 & 0 & 0 \\ 1 & 1 & 1 \end{bmatrix} \quad \begin{bmatrix} -1 & 0 & 1 \\ -1 & 0 & 1 \\ -1 & 0 & 1 \end{bmatrix}$$

Vertical Horizontal

$$\begin{bmatrix} 0 & -1 & -1 \\ 1 & 0 & -1 \\ 1 & 1 & 0 \end{bmatrix} \quad \begin{bmatrix} -1 & -1 & 0 \\ -1 & 0 & 1 \\ 0 & 1 & 1 \end{bmatrix}$$

45° 135°

The Prewitt operators

$$\begin{bmatrix} -1 & -2 & -1 \\ 0 & 0 & 0 \\ 1 & 2 & 1 \end{bmatrix} \quad \begin{bmatrix} -1 & 0 & 1 \\ -2 & 0 & 2 \\ -1 & 0 & 1 \end{bmatrix}$$

Vertical Horizontal

$$\begin{bmatrix} 0 & -1 & -2 \\ 1 & 0 & -1 \\ 2 & 1 & 0 \end{bmatrix} \quad \begin{bmatrix} -2 & -1 & 0 \\ -1 & 0 & 1 \\ 0 & 1 & 2 \end{bmatrix}$$

45° 135°

The Sobel operators

Edge Detection in Digital Images

- The Laplacian is a second-order difference operator, widely used for omnidirectional edge detection.

$$\begin{bmatrix} 0 & 1 & 0 \\ 1 & -4 & 1 \\ 0 & 1 & 0 \end{bmatrix}$$

- The Laplacian produces double-edged outputs, and is sensitive to noise.
- The Laplacian-of-Gaussian (LoG) is the combination of the Laplacian and the Gaussian, and can be used for robust omnidirectional edge detection.

Canny's Method for Edge Detection

- Optimal edge detection technique.
- Based upon three criteria for good edge detection:
  - multi-directional derivatives,
  - multi-scale analysis, and
  - optimization procedures.
- Selectively evaluates directional derivatives at each edge.

Canny's Method for Edge Detection

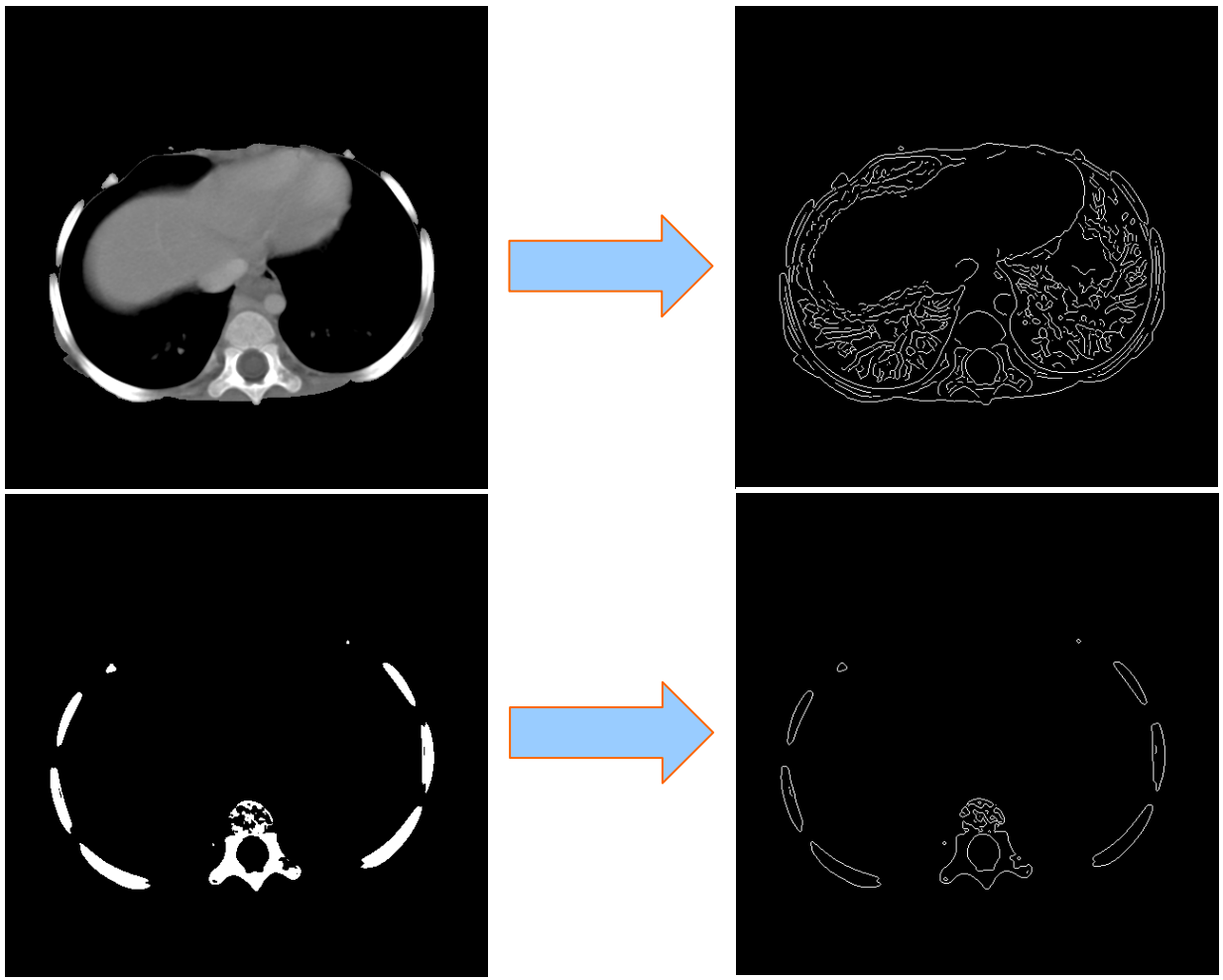

Image Segmentation Using Deformable Contours (Snakes)

- Contour in image domain that deforms according to internal and external forces.
- Internal forces are defined within the contour itself to maintain the contour smooth.
- External forces are computed from the image data to move the contour toward an object boundary.
- When the external and the internal forces become equal, the force field attains equilibrium and the contour stabilizes.

Deformable Contours

- Modeled as a closed curve:

$$C(s) = (X(s), Y(s)), s \in [0,1]$$

- The contour is like an elastic string subjected to a set of dynamic forces:

$$\mu_m \frac{\partial^2 \mathbf{C}}{\partial t^2} = \mathbf{F}_{\text{int}}(\mathbf{C}) + \mathbf{F}_{ext}(\mathbf{C}) + \mathbf{F}_{damp}(\mathbf{C})$$

μ_m : specific mass of the contour; t : time

Deformable Contours

- The Internal force is given by:

$$\mathbf{F}_{\text{int}}(\mathbf{C}) = \frac{\partial}{\partial s}\left(\alpha \frac{\partial \mathbf{C}}{\partial s}\right) - \frac{\partial^2}{\partial s^2}\left(\beta \frac{\partial^2 \mathbf{C}}{\partial s^2}\right)$$

α : tension; β : rigidity

- The 1st order derivative discourages stretching, and makes the model behave like an elastic string.

- The 2nd order derivative discourages bending, and makes the model behave like a rigid rod.

Deformable Contours

- The damping (viscous) force is given by:

$$\mathrm{F}_{damp}(\mathrm{C}) = -\gamma \frac{\partial \mathrm{C}}{\partial t}; \qquad \gamma : \text{viscosity}$$

- A viscous force is introduced to stabilize the deformable contour around the static equilibrium configuration.

- The mass of the contour is often assumed to be zero:

$$\gamma \frac{\partial \mathbf{C}}{\partial t} = \mathbf{F}_{\text{int}}(\mathbf{C}) + \mathbf{F}_{ext}(\mathbf{C})$$

Deformable Contours

- The external force can be composed of either potential forces or non-potential forces.
- Traditional definition of external force for image $I(x,y)$:

$$\mathbf{F}_{ext}(\mathbf{C}) = -\nabla\left|\nabla I(x,y)\right|^2$$

- If the contour is not initialized close to the object's boundary, the external force will have a low intensity and will not result in proper convergence.
- To address this problem Gradient Vector Flow (GVF) field could be used as an external force.

Gradient Vector Flow (GVF)

- Based on a vector diffusion equation that diffuses the gradient of an edge map in regions distant from the boundary.

- GVF field $[u(x,y), v(x,y)]$ is defined as the solution to

$$\lambda\nabla^2 u - \left(u - \frac{\partial E}{\partial x}\right)\left(\left(\frac{\partial E}{\partial x}\right)^2 + \left(\frac{\partial E}{\partial y}\right)^2\right) = 0$$

$$\lambda\nabla^2 v - \left(v - \frac{\partial E}{\partial x}\right)\left(\left(\frac{\partial E}{\partial x}\right)^2 + \left(\frac{\partial E}{\partial y}\right)^2\right) = 0$$

where $E(x,y) = \left|\nabla I(x,y)\right|^2$, λ is a regularization parameter.

Gradient Vector Flow (GVF)

The spatial extent of the external forces may be enhanced with the mapping function:

$$f(\mathbf{w}(x,y)) = K_2\left[1-\exp\left(\frac{-\mathbf{w}(x,y)}{K_1}\right)\right]\frac{\mathbf{w}(x,y)}{\left|\mathbf{w}(x,y)\right|}$$

where $\mathbf{w}(x,y) = \left[u(x,y) \;\; v(x,y)\right]^T$, the GVF field component;

K_1 determines the rate of convergence

K_2 determines the asymptote of convergence

Image Segmentation Using Deformable Contours (Snakes)

$$\alpha = 30, \beta = 10, \lambda = 0.1, K_1 = 0.1, K_2 = 1.0$$

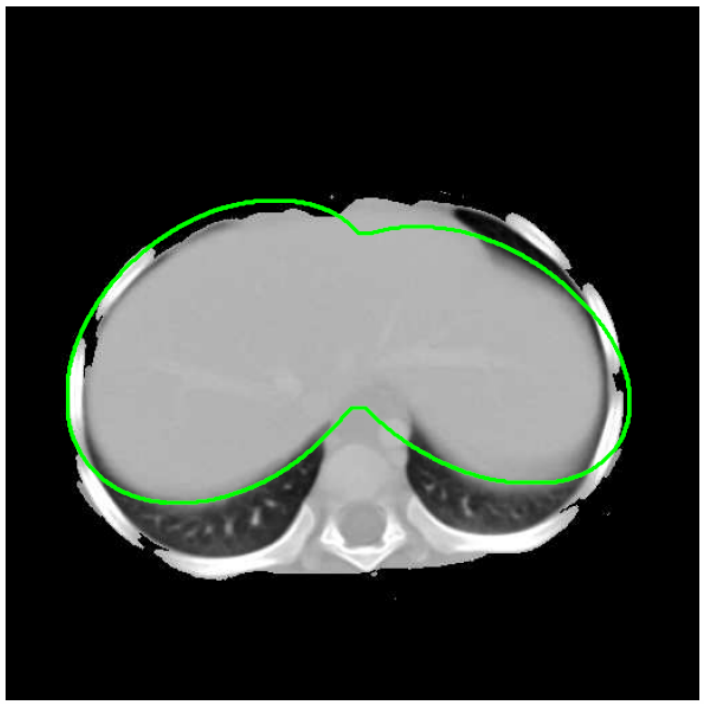

automatic initialization

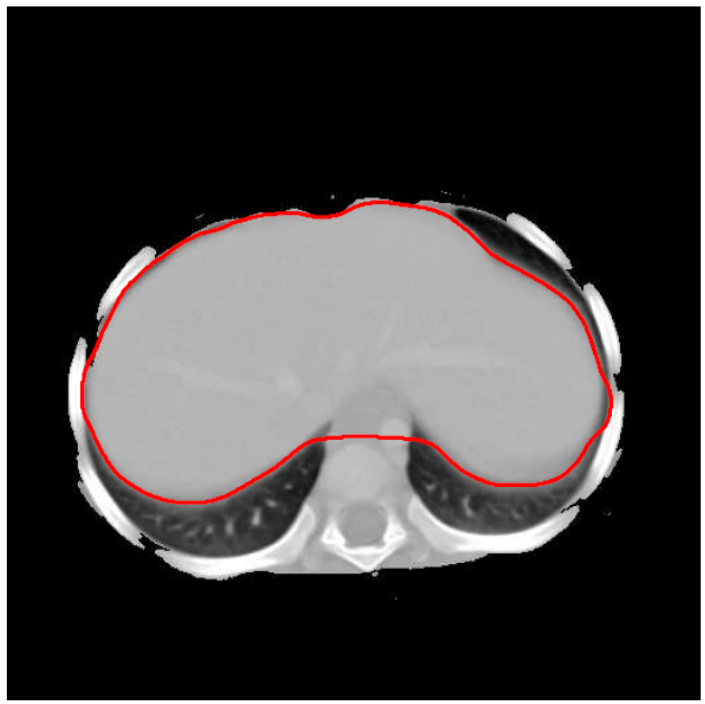

contour of the diaphragm

The Hough Transform

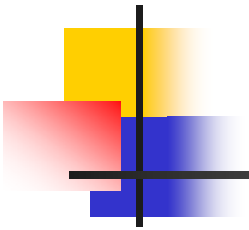

- Useful tool to detect any shape that can be represented by a parametric equation (straight line, circle, ellipse).
- Uses the information related to the edges in the form of a binary image.
- Has the ability to recognize shapes and object boundaries, even with sparse edge map.

The Hough Transform

Detection of straight lines:

- A straight line can be represented by the angle θ of its normal and its distance ρ from the origin by the equation

$$\rho = x\cos\theta + y\sin\theta$$

- In the Hough space or parameter space (ρ, θ), any straight line in the image domain is represented by a single point.

- The sinusoidal curves in the parameter space of all points that lie on the line $\rho_0 = x\cos\theta_0 + y\sin\theta_0$ intersect at (ρ_0, θ_0).

The Hough Transform

Detection of straight lines:

- θ is restricted to [0º, 180º] or [0º, 360º].
- ρ is restricted by the size of the image.
- The origin may be chosen at the center of the image or any arbitrary point.
- The value of ρ can be considered to be negative for normals to lines extending below the horizontal axis, $x=0$, in the image, with the origin at the center of the image, and θ in the range [0º, 180º].

The Hough Transform

Detection of straight lines:

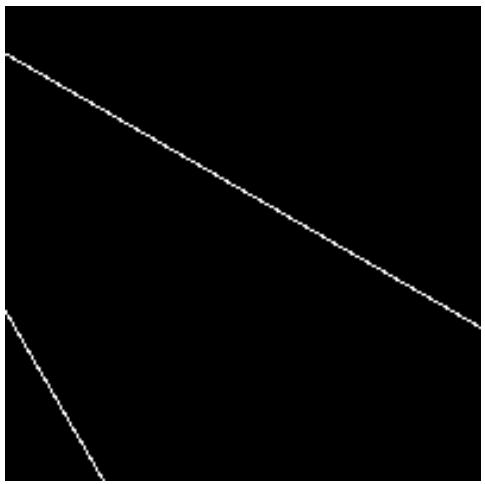

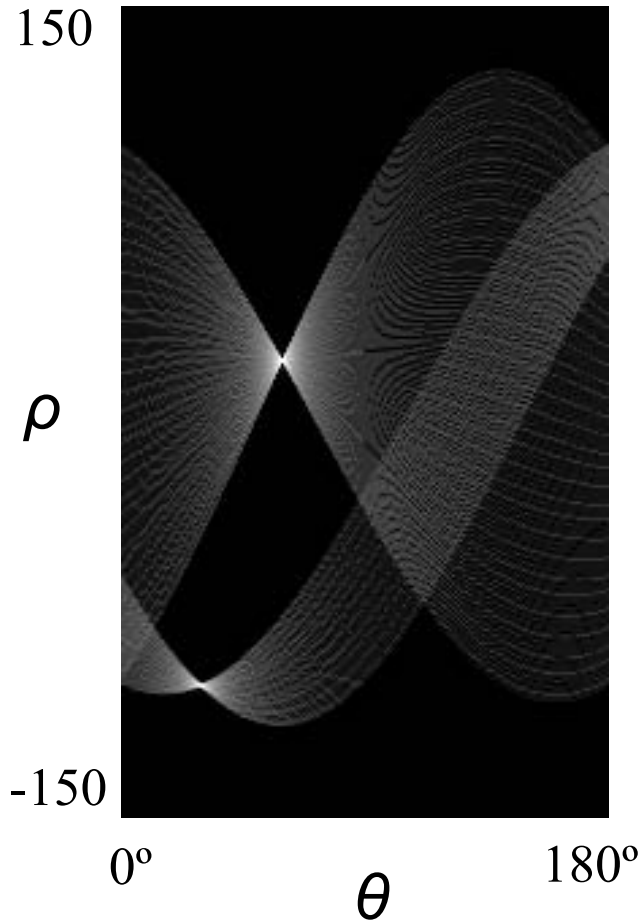

An image with two straight lines
(ρ, θ)=(-100, 30º) and (20, 60º).
Limits of x and y axis are ±100;
the origin is at the center of the image.

The Hough Transform

Detection of circles:

- All points along the circumference of a circle of radius c centered at $(x, y) = (a, b)$ satisfy the relationship

$$(x-a)^2 + (y-b)^2 = c^2$$

- A circle is represented by a single point in the 3D parameter space (a, b, c).
- The points along the circumference or the edge of a circle in the (x, y) plane describe a right circular cone in the Hough parameter space, which is limited by the image size.

The Hough Transform

Detection of circles:

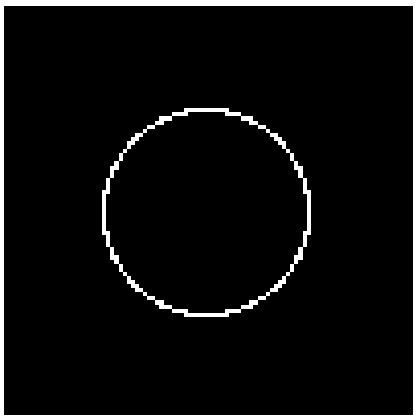

100×100 image, with a circle of radius $c = 25$ pixels, centered at $(x, y) = (50, 50)$. $(x, y) = (1, 1)$ is at the top left corner.

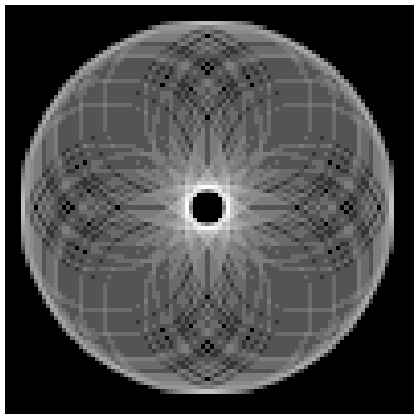

$c = 20$ pixels

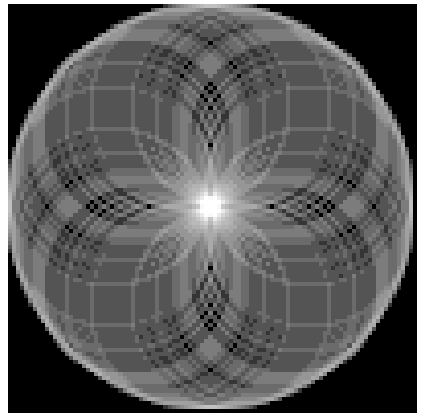

$c = 24$ pixels

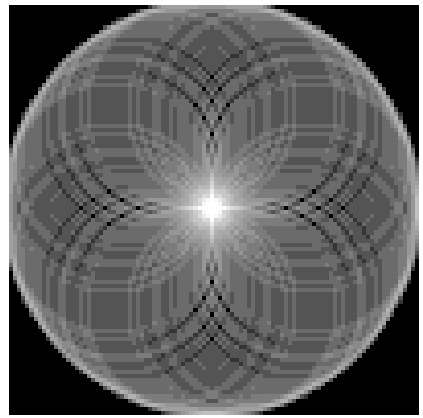

$c = 25$ pixels

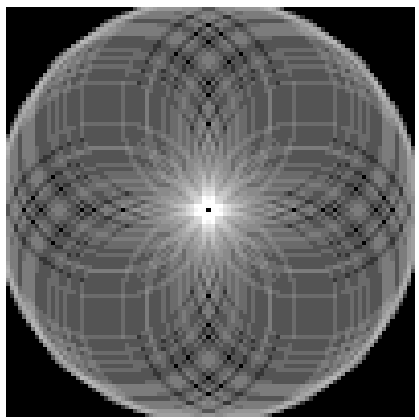

$c = 26$ pixels

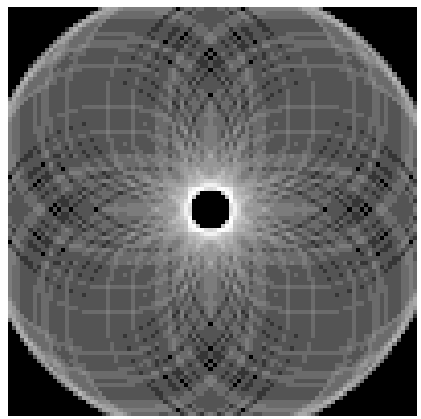

$c = 30$ pixels

The Convex Hull

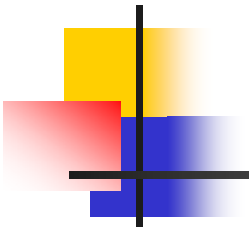

- The convex hull H of a set of points S is the smallest convex set that contains all the points.

- A set A is said to be convex if the straight-line segment joining any two points in A lies entirely within A.

- The set difference $H - S$ is called the convex deficiency of S.

The Convex Hull

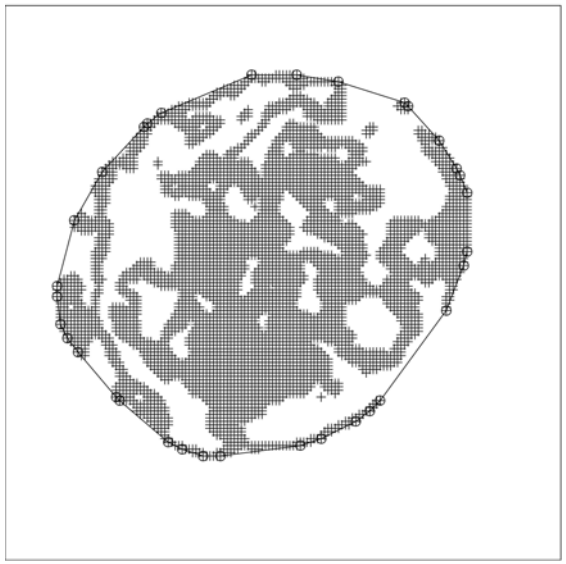

Convex hull

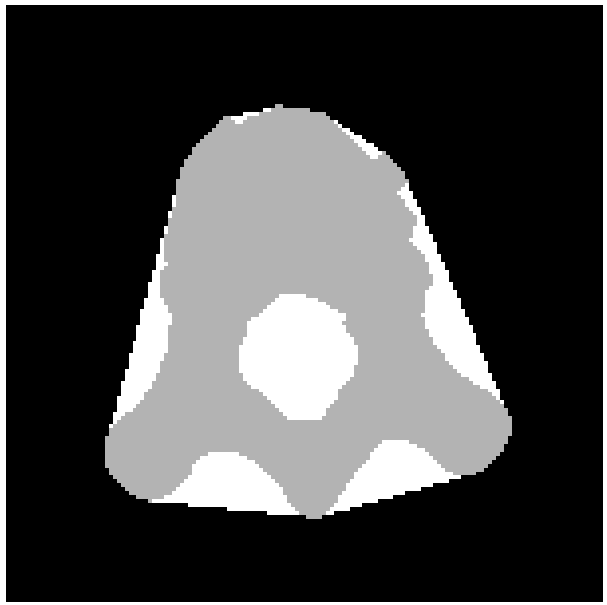

Gray: actual region

White: convex deficiency

Fuzzy Sets

A fuzzy set $\boldsymbol{A}$ in a reference set $\boldsymbol{X}$ can be characterized by a membership function, $m_{\boldsymbol{A}}$, that maps all elements in $\boldsymbol{X}$ into the interval $[0, 1]$.

The fuzzy set may be represented as a set of fuzzy pairings

$$\boldsymbol{A} = \{(x, m_{\boldsymbol{A}}(x)) \mid x \in \boldsymbol{X}\}$$

$$m_{\boldsymbol{A}}(x) = x \rightarrow [0, 1], \text{ for } x \in \boldsymbol{X}$$

The membership value $m_{\boldsymbol{A}}(x)$ denotes the degree to which an element x satisfies the properties of the set $\boldsymbol{A}$.

Fuzzy Sets

Given two fuzzy sets $\boldsymbol{A}$ and $\boldsymbol{B}$ with the membership functions $m_{\boldsymbol{A}}(x)$ and $m_{\boldsymbol{B}}(x)$, the standard set-theoretic relations and operations are defined as:

Equality (=): $\boldsymbol{A} = \boldsymbol{B} \Leftrightarrow m_{\boldsymbol{A}} = m_{\boldsymbol{B}}$

Containment ($\subset$): $\boldsymbol{A} \subset \boldsymbol{B} \Leftrightarrow m_{\boldsymbol{A}} \leq m_{\boldsymbol{B}}$

Complement (~): $m_{\tilde{\boldsymbol{A}}}(x) = 1 - m_{\boldsymbol{A}}(x)$

Intersection ($\cap$): $m_{\boldsymbol{A} \cap \boldsymbol{B}}(x) = \min \{m_{\boldsymbol{A}}(x), m_{\boldsymbol{B}}(x)\}$

Union (U): $m_{\boldsymbol{A} \cup \boldsymbol{B}}(x) = \max \{m_{\boldsymbol{A}}(x), m_{\boldsymbol{B}}(x)\}$

Fuzzy Mapping

- The value $m_A(r)$ is called the *grade of membership* of r in A: this function indicates the degree to which r satisfies the membership criteria defining A.
- Consider the set of numbers that are “close to 10”. In defining $m_A(r)$, three properties should be satisfied:

  1. *Normality*: $m_A(10) = 1$.
  2. *Monotonicity*: the closer the value of r is to 10, the closer m_A should be to 1.
  3. *Symmetry*: numbers equally far from 10, such as 9 and 11, should have equal membership.

Fuzzy Mapping

The unnormalized Gaussian function, defined as

$$m_A(r) = \exp\left\{-\frac{(r-\mu)^2}{2\sigma^2}\right\}$$

satisfies all the properties.

The parameters μ and σ characterize the set A.

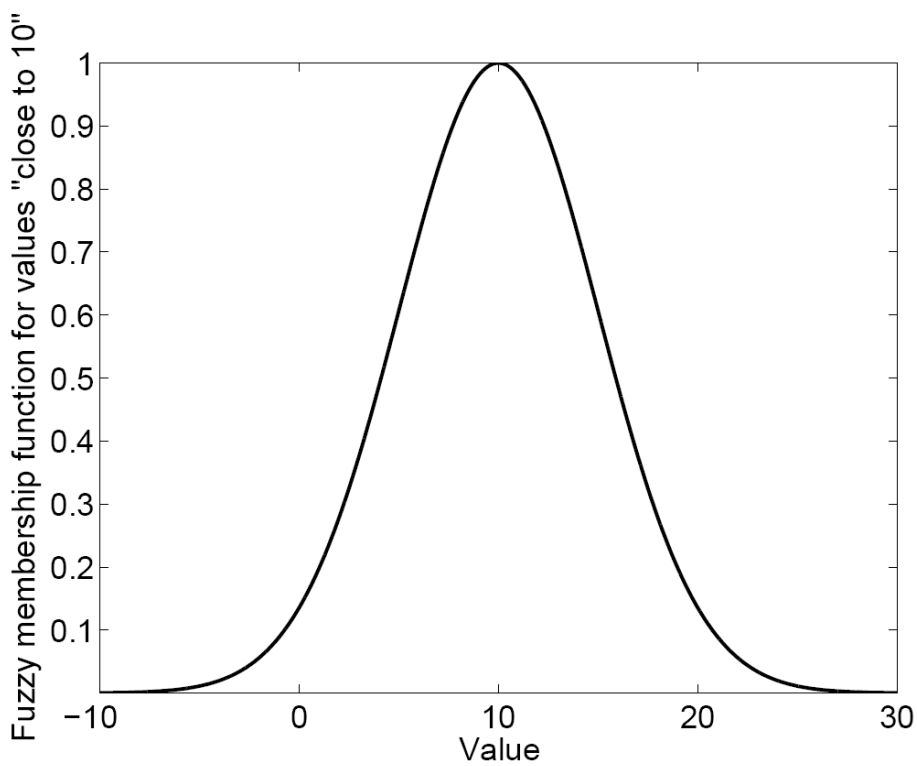

Fuzzy Mapping

Original image

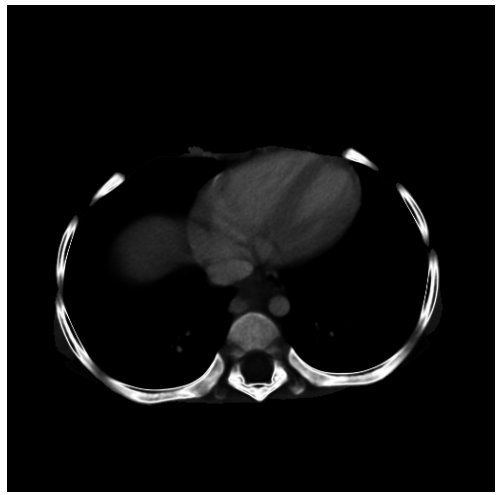

μ = 412 HU, σ = 156 HU

μ = -528 HU, σ = 121 HU

μ = 18 HU, σ = 14 HU

Fuzzy Connectivity: Affinity

- Object definition is based on local affinity between voxels as proposed by Udupa and Samarasekera.
- The closer the voxels and the more similar their values, the greater the affinity

$$\eta(a,b) = \exp\left\{-\frac{1}{2}\left[\frac{\left(\frac{f(a)+f(b)}{2}\right)-\mu}{\sigma}\right]^2\right\}$$

a and b are two adjacent (six-connected) voxels.

μ = mean of 3 x 3 x 3 region surrounding the seed voxel, σ = SD

Fuzzy Connectivity: Connectedness

- Connectedness is based on the affinity function.
- The connectedness is dependent on all possible connecting paths between two voxels.
- A connecting path is formed from a sequence of links between successive adjacent voxels in the path.
- The strength of each link is the affinity between the two adjacent voxels in the link.
- The strength of a path is the strength of its weakest link.

Fuzzy Connectivity: Connectedness

- The strength of connectedness between two voxels is the strength of the strongest path.
- The points belonging to the same object should possess a high degree of connectedness due to
  - the strong resemblance based on the fuzzy membership, and
  - the existence of strong paths connecting them.

Fuzzy Connectivity: Connectedness

- Background or undesired elements should possess a low degree of connectedness with the object.
- Paths could exist between the desired and undesired elements: they would possess low membership values.

Fuzzy Connectivity: Algorithm

- Initialize algorithm with seed voxel; assign the maximum membership of unity.
- Grow region by evaluating the connectivity between the seed voxel and all connected voxels in the volume.
- Produce membership volume.
- Threshold membership volume to obtain hard binary segmentation.

Morphological Image Processing

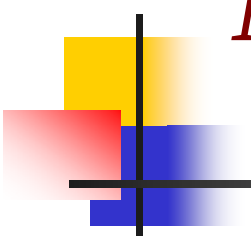

- A branch of nonlinear image processing that concentrates on the analysis of geometrical structures in an image.
- Based on conventional set theory.
- Probe the image with the *structuring element* and quantify the manner in which the structuring element fits, or does not fit, within the image.
- The most elementary set operations relating to mathematical morphology should be *increasing* and *translation invariant*.

Binary Morphological Image Processing

- Fundamental binary operations are based on *Minkowski algebra.*
- Fundamental operations are:
  - erosion, and
  - dilation.
- Secondary operations are:
  - opening (erosion + dilation), and
  - closing (dilation + erosion).

Erosion

- Translation invariant, known as *Minkowski subtraction.*
- If the origin lies within the structuring element, the effect is shrinking; the result is a subset of the original image.
- Protrusions smaller than the structuring element are eliminated.
- In digital implementation, if any of the pixels within the neighborhood defined by the structuring element is ‘off’ (i.e., set to 0), the output pixel is also set to 0.

Erosion

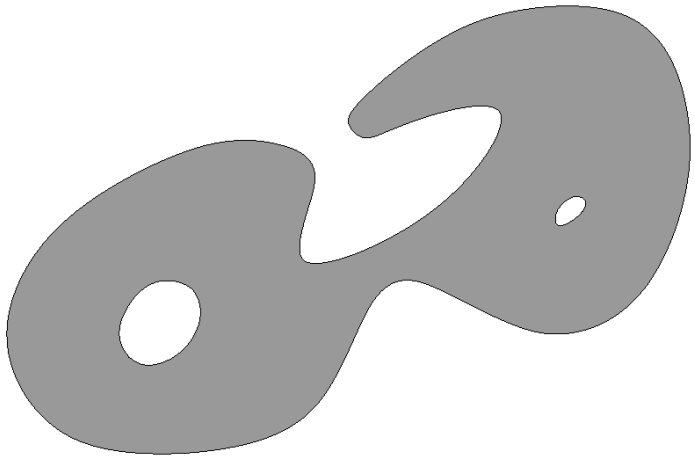

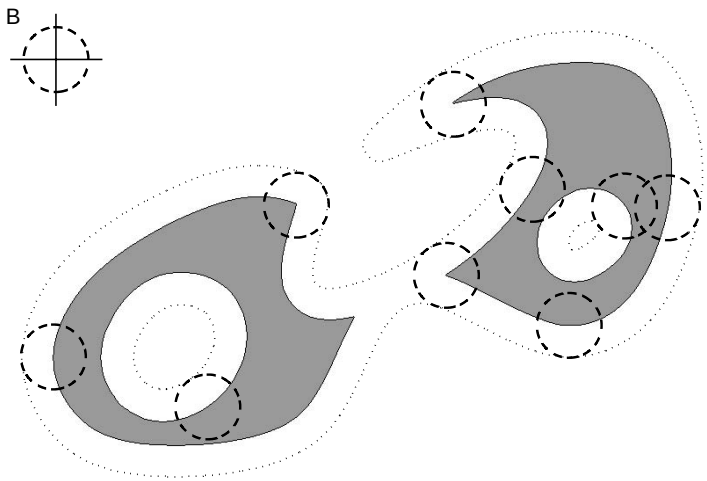

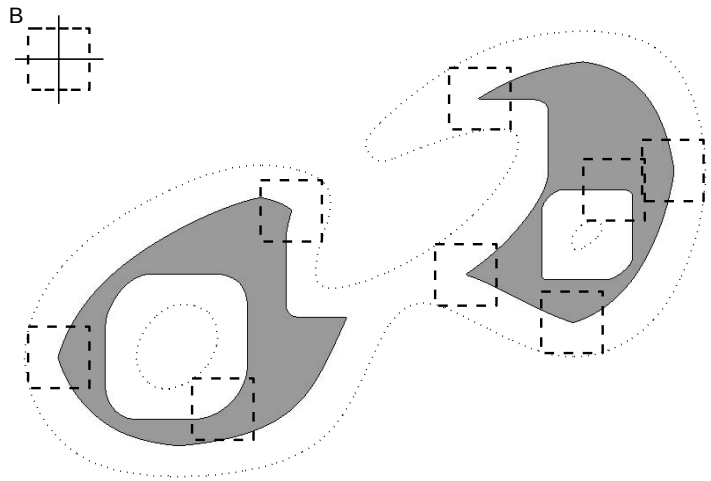

Dilation

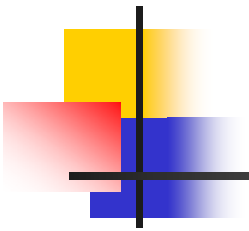

- Translation invariant, known as *Minkowski addition.*
- If the origin lies within the structuring element, it fills in small holes (relative to the structuring element) and intrusions.
- Represents filtering on the outside, and has the effect of expansion.
- In digital implementation, if any of the pixels within the neighborhood defined by the structuring element is ‘on’ (i.e., set to 1), the output pixel is also set to 1.

Dilation

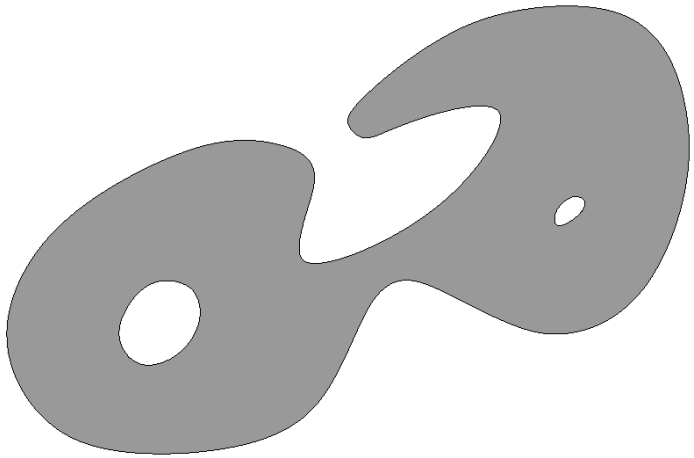

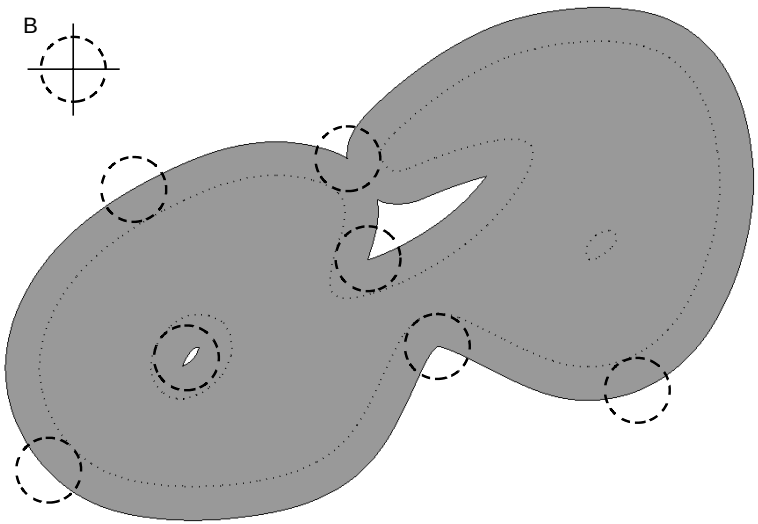

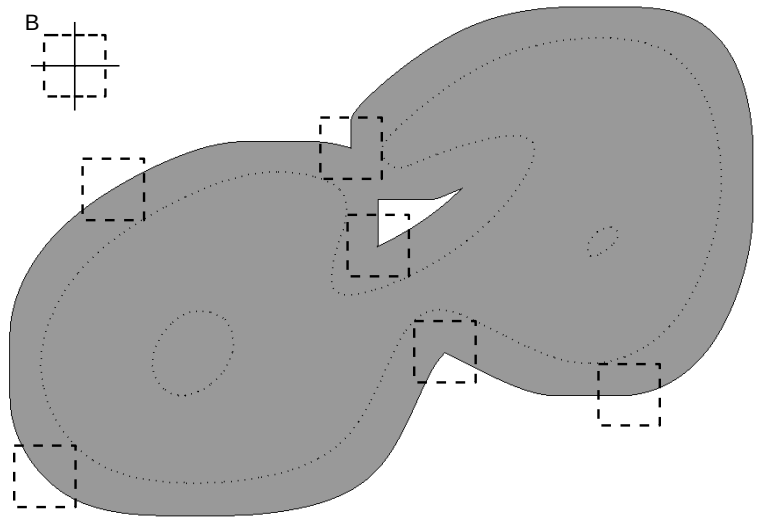

Opening

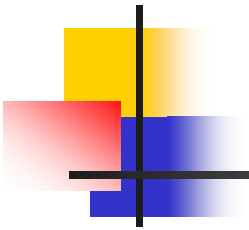

- Has the property of idempotency.
- Obtained by applying erosion followed by dilation.
- If the origin lies within the structuring element:
  - removes objects smaller than the structuring element,
  - smoothens the edges of the remaining objects, and
  - disconnects objects that are connected by branches smaller than the structuring element.

Opening

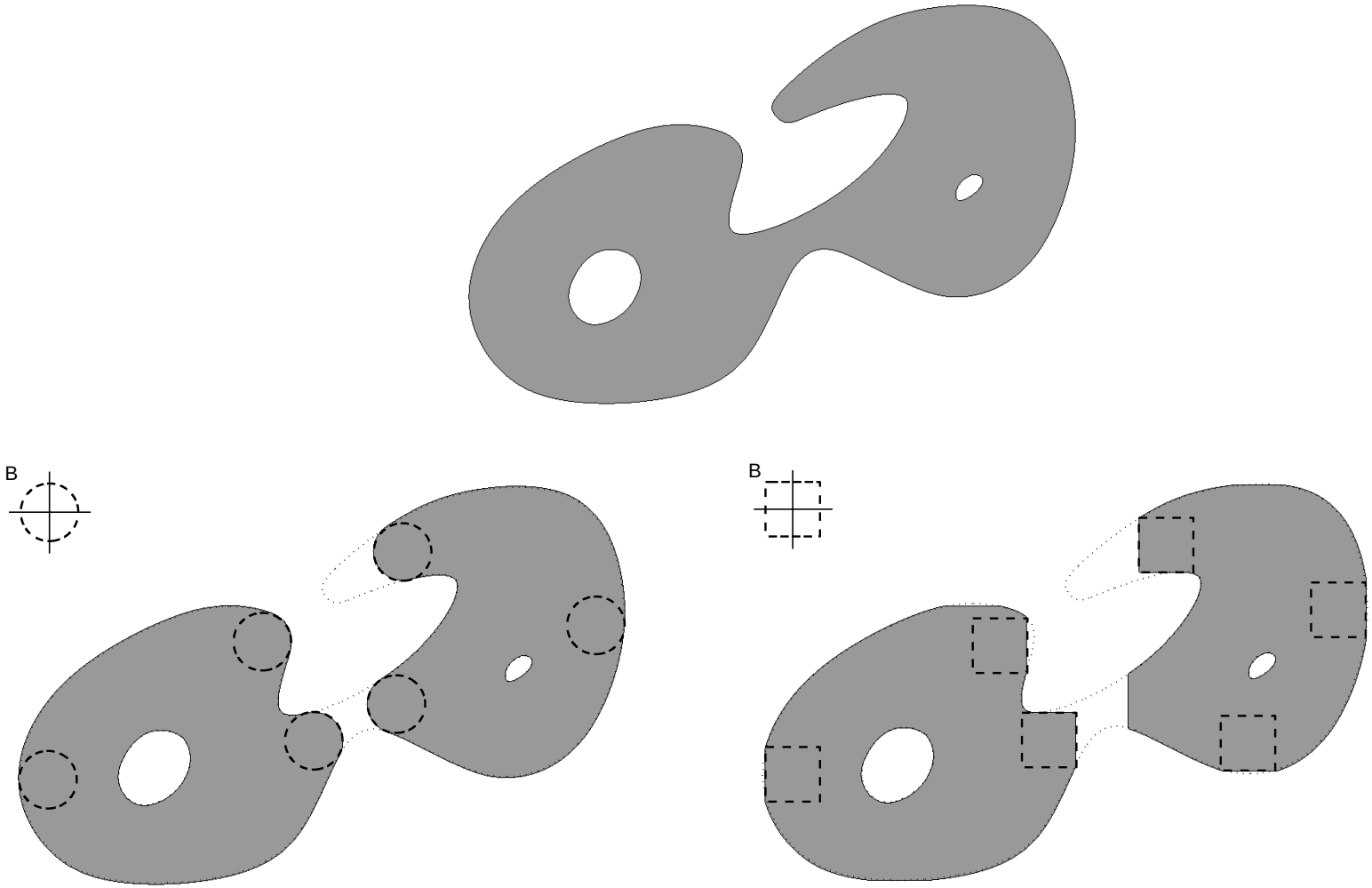

Closing

- Has the property of idempotency.
- Obtained by applying dilation followed by erosion.
- If the origin lies within the structuring element:
  - fills in holes and intrusions smaller than the structuring element, and
  - connects objects that are disconnected by gaps smaller than the structuring element.

Closing

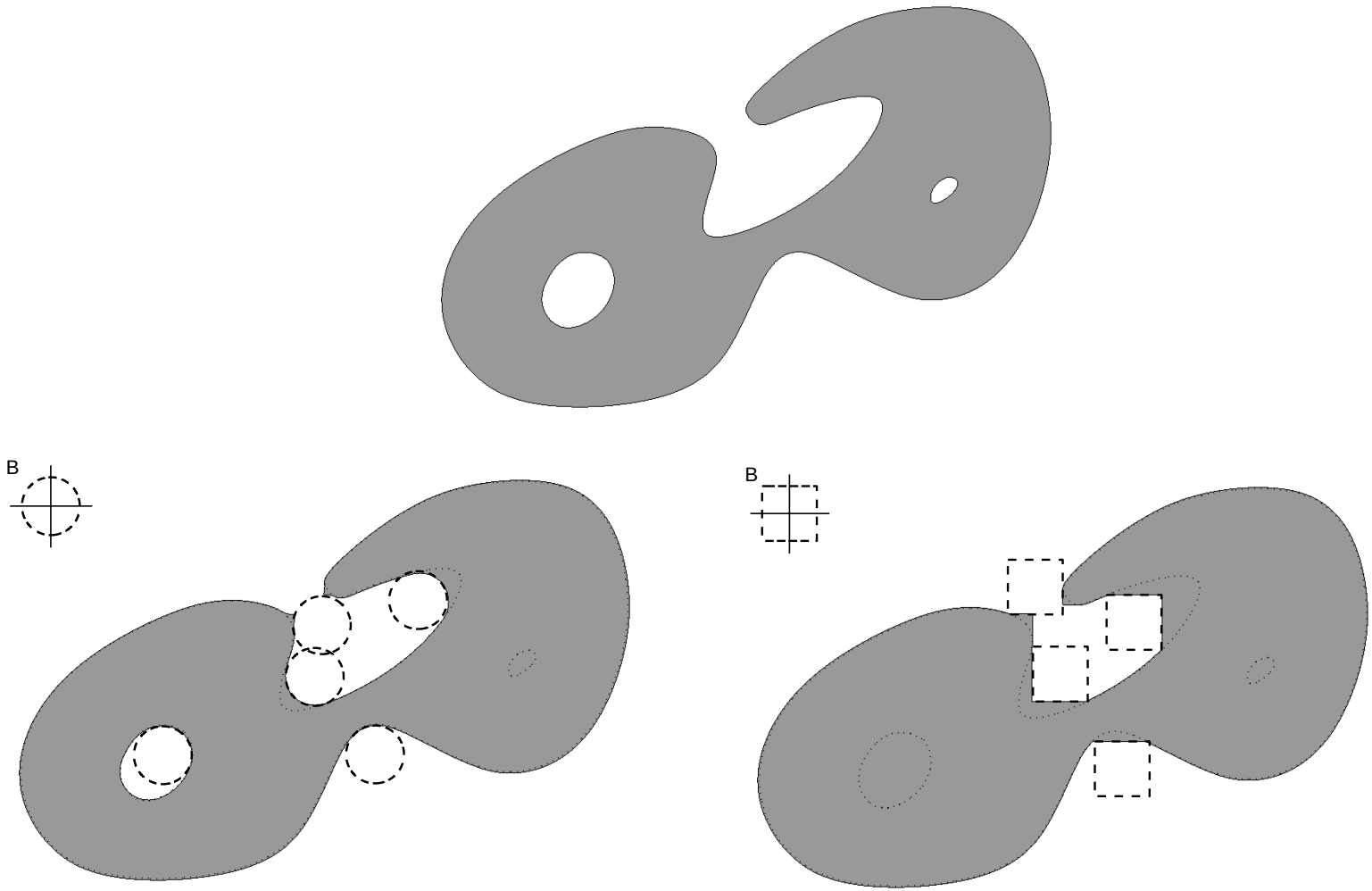

Binary Morphological Operations

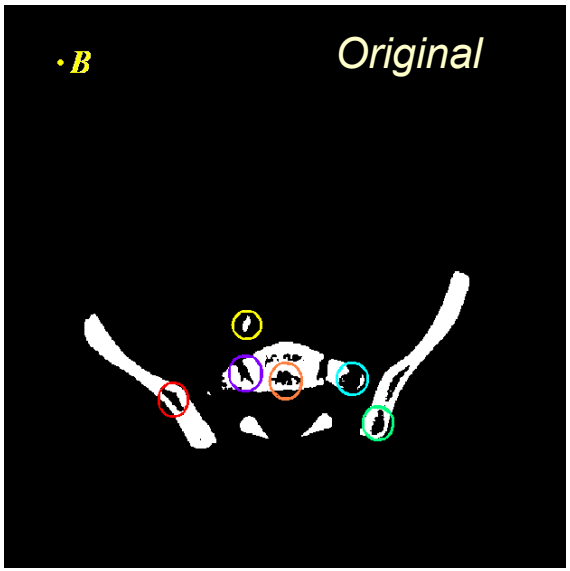

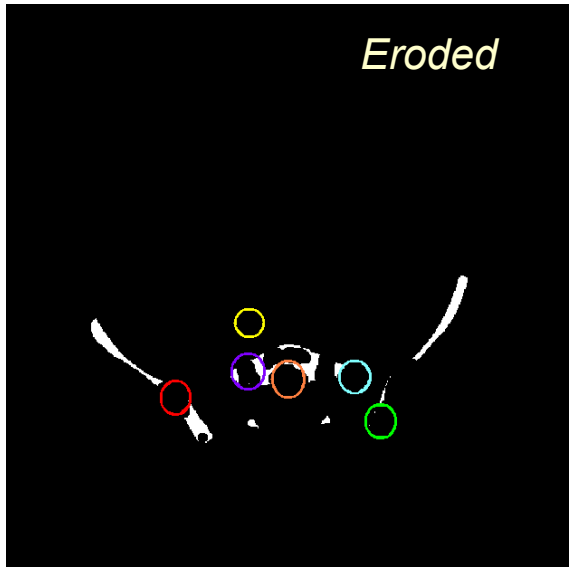

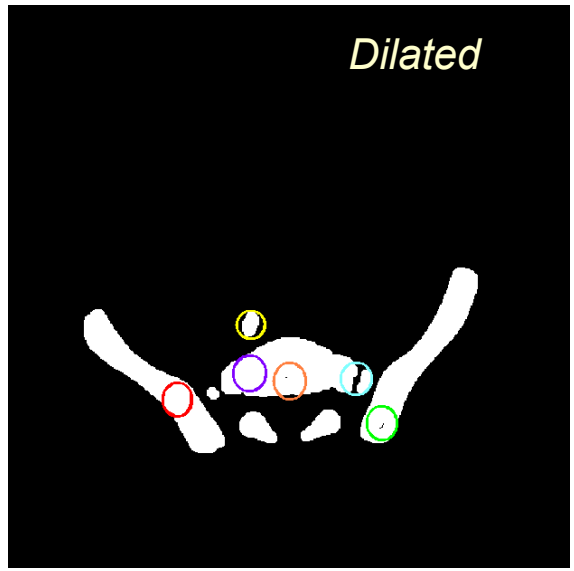

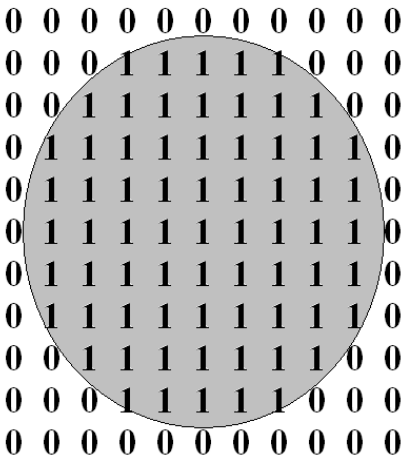

Disk-type flat structuring element of radius 5 pixels

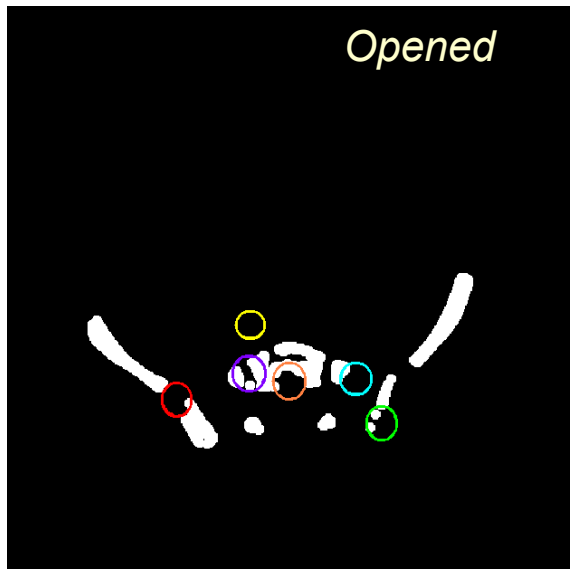

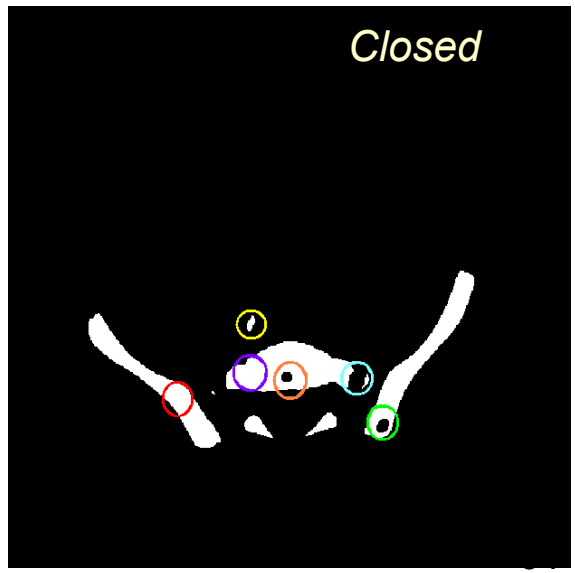

Gray-scale Morphological Image Processing

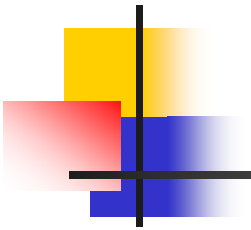

- Extension of binary morphological image processing using *threshold decomposition*: decomposing a gray-scale image into a series of "stacked" binary images.
- Gray-scale flat erosion: replaces the value of an image f at a pixel (x, y) by the infimum of the values of f over the structuring element B.
- Gray-scale flat dilation: replaces the value of an image f at a pixel (x, y) by the supremum of the values of f over the reflected structuring element $\check{B}$.
- Gray-scale opening and closing obtained similarly.

Opening-by-reconstruction

- Morphological operator that analyzes the connectivity of objects in the image.
- Iterative procedure to extract regions of interest from the image using a ‘marker’.
- Computationally more efficient than fuzzy connectivity: useful for multi-seed approach.

Opening-by-reconstruction

Starting with a mask, I, and marker, J, the gray-scale reconstruction, ρ_I, is defined as

$$\rho_I(J) = \bigvee_{n \geq 1} \delta_I^{(n)}(J)$$

where $\delta_I^{(n)}$ refers to n iterations of geodesic dilation and $\vee$ represents the supremum of the results.

Opening-by-reconstruction

Marker, J, is dilated using a structuring element, B, such that result is constrained to the mask, $I \rightarrow J \subseteq I$.

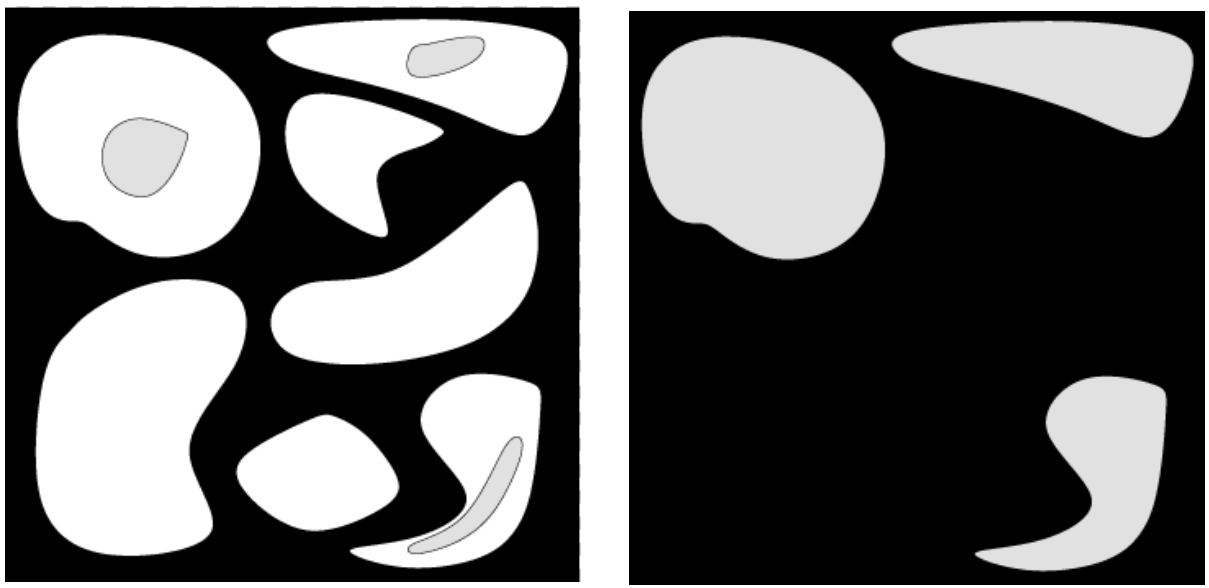

Image Segmentation Using Opening-by-reconstruction

- Image mapped to obtain fuzzy-membership values:

$$f(x,\mu,\sigma) = \exp\left(-\frac{(x-\mu)^2}{2\sigma^2}\right)$$

- Using this mapping, elementary dilations performed on the marker, restricted by the mask.

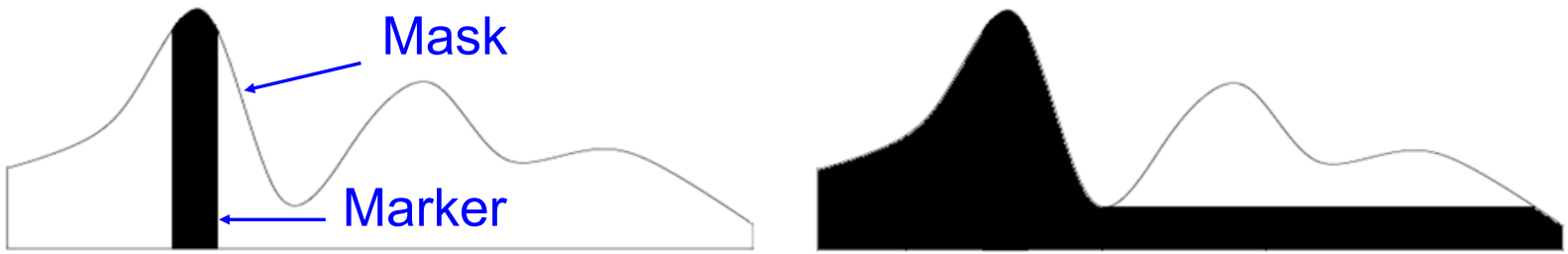

Image Segmentation Using Opening-by-reconstruction

- Mask = fuzzy-membership map (constraint)
- Marker = seed pixel or region (starting point)
- Dilate marker within the mask until no further change is found between two iterations.

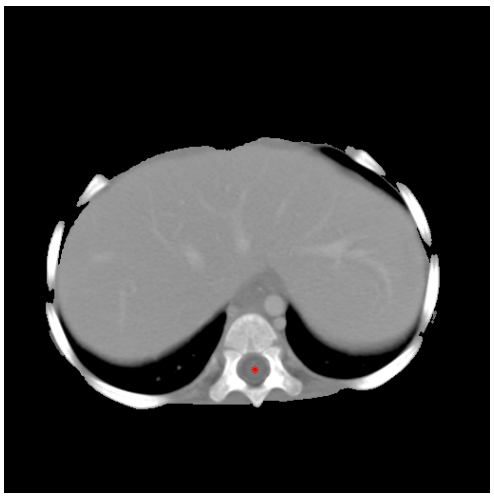

seed pixel

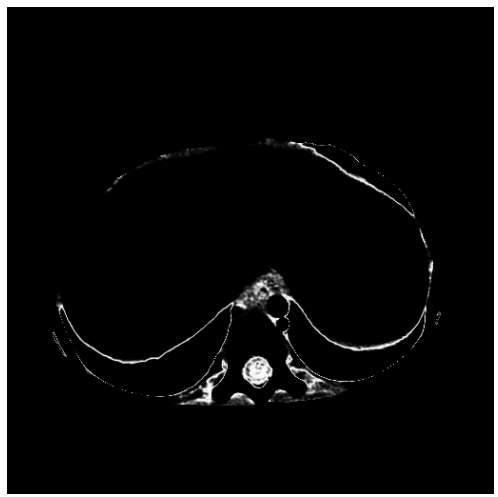

fuzzy-map
(μ = 30 HU, σ =17 HU)

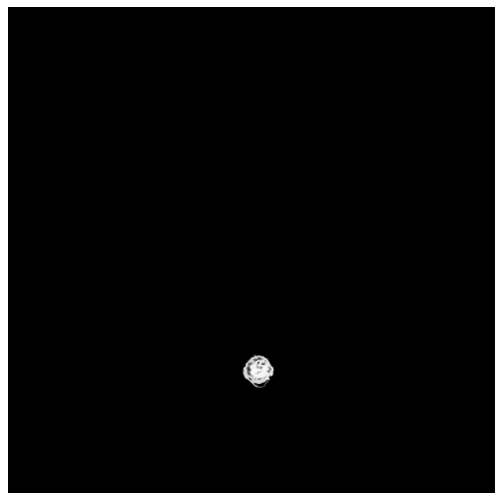

result

Linear Least-squares (LLS) Estimation

- Extract N coordinates of the surface and place in a vector:

$$\mathbf{v}_i = \left(x_i, y_i, z_i\right)$$

- Model the expected region as a quadratic surface:

$$z_i' = a_0 x_i^2 + a_1 y_i^2 + a_2 x_i y_i + a_3 x_i + a_4 y_i + a_5$$

- Calculate error between real data, $\mathbf{z}$, and model, $\mathbf{z'}$:

$$\mathbf{r} = \mathbf{z} - \mathbf{z}'$$

Linear Least-squares (LLS) Estimation

- Estimate the best set of parameters

$$\hat{\mathbf{a}} = (\mathbf{\Omega}^T \mathbf{\Omega})^{-1} \mathbf{\Omega}^T \mathbf{z}$$

that minimizes the squared error $\mathbf{r}^T\mathbf{r}$ where

$$\mathbf{\Omega} = \begin{bmatrix} x_1^2 & y_1^2 & x_1 y_1 & x_1 & y_1 & 1 \\ x_2^2 & y_2^2 & x_2 y_2 & x_2 & y_2 & 1 \\ \vdots & \vdots & \vdots & \vdots & \vdots & \vdots \\ x_N^2 & y_N^2 & x_N y_N & x_N & y_N & 1 \end{bmatrix}$$

CT Dataset

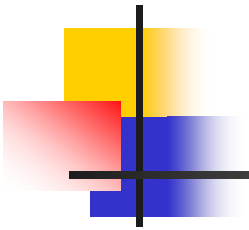

- Number of patients: 14
- Number of CT exams: 40
- Ages of the patients: 2 weeks to 20 years
- Intra-slice resolution: 0.35 mm to 0.70 mm
- Inter-slice resolution: 2.5 mm or 5 mm
- Number of exams including contrast: 36

Quantitative Assessment

- Hausdorff distance: The directed Hausdorff distance

from set A to set B is defined as

$$h(A, B) = \max_{a \in A} \left[\min_{b \in B} \{ d(a, b) \} \right]$$

A more general definition of the Hausdorff distance:

$$H(A, B) = \max\{ h(A, B), h(B, A) \}$$

Quantitative Assessment

- Mean Distance to the Closest Point (MDCP):

Given two sets $A = \{a_1, a_2, \ldots, a_M\}$ and $B = \{b_1, b_2, \ldots, b_N\}$

distance to the closest point (DCP) is defined as

$$\mathrm{DCP}\,(a_i, B) = \min ||a_i - b_j||, \quad j = 1, 2, \ldots, N$$

$$\mathrm{MDCP}\,(A, B) = \frac{1}{M} \sum_{i=1}^{M} \mathrm{DCP}\,(a_i, B)$$

Quantitative Assessment

- Measures of volumetric accuracy:
  - Total error $$\varepsilon_T = \frac{V(A) - V(R)}{V(R)} \times 100\%.$$
  - False-positive error rate $$\varepsilon_{FP} = \frac{V(A) - (V(A) \cap V(R))}{V(R)} \times 100\%$$
  - True-positive rate $$\varepsilon_{TP} = \frac{V(A) \cap V(R)}{V(R)} \times 100\%$$

where V () is the volume, A is the result of segmentation using the proposed procedures, and R is the result of segmentation by a radiologist (the ground truth).

Preprocessing Steps

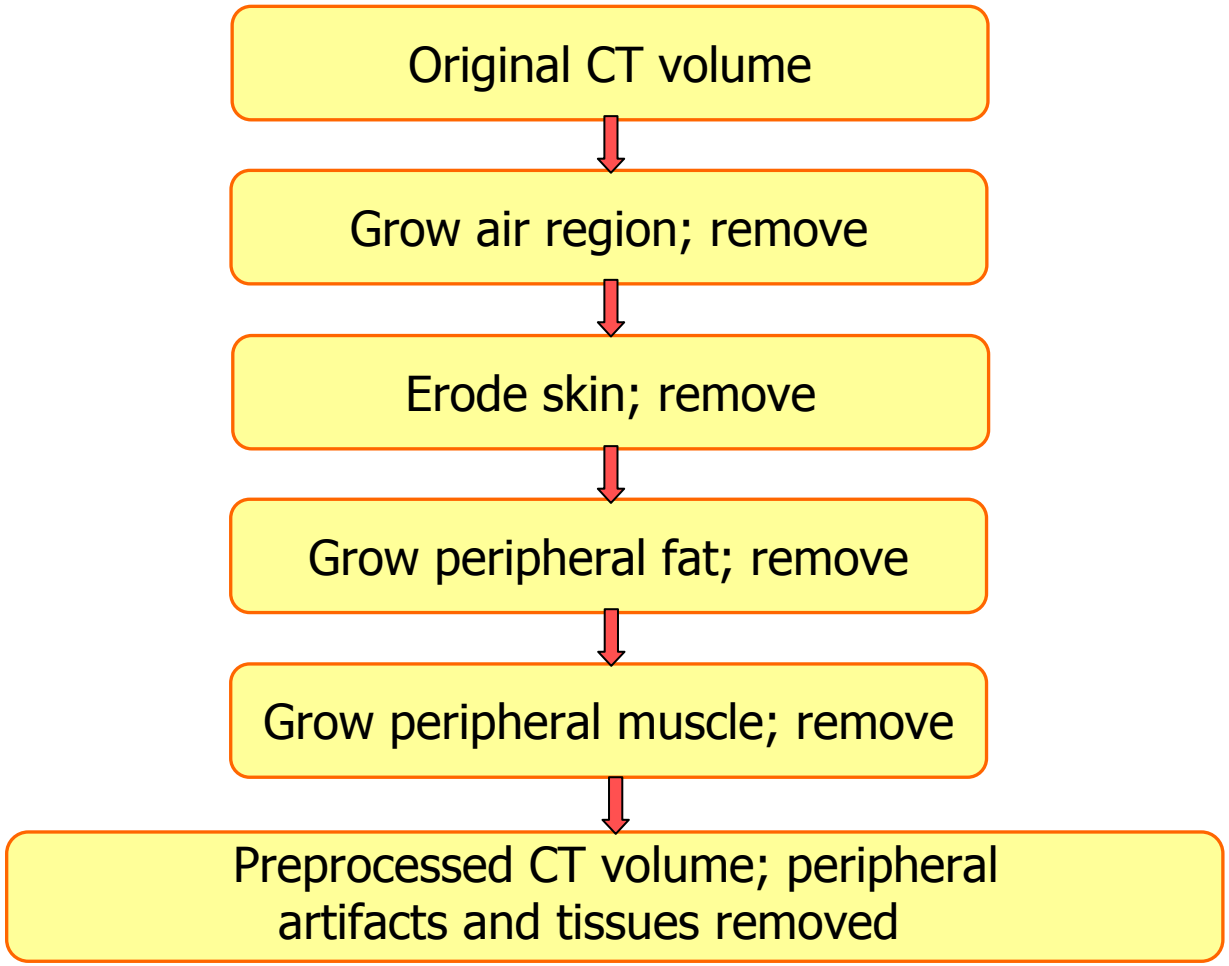

Removal of Peripheral Artifacts and the External Air Region

- By definition, air has CT number of –1000 HU.
- Each CT volume is thresholded with the range -1200 HU to -400 HU.
- 2D binary opening-by-reconstruction is applied on a slice-by-slice basis using the thresholded volume as mask and the four corners of each slice as markers.
- Morphologically closed using a disk type structuring element of radius 10 pixels (approximately 5 mm) to remove material external to the body.

Removal of the Skin Layer

- Skin is the first layer from the outside of the body, with usual thickness of 1 to 3 mm.
- The air region is morphologically dilated in 2D to include the skin.
- The skin layer could be used as a landmark for registration and segmentation.

Removal of the Peripheral Fat

- The peripheral fat is the next layer after the skin from the outside of the body; varies in thickness from 3 to 8 mm in children.
- Fat has a mean CT value of μ = -90 HU with σ =18 HU.
- Voxels within a distance of 8 mm from the inner skin boundary are examined; if they fall within the range -90 ± 2 × 18 HU, they are classified as peripheral fat.

Removal of the Peripheral Muscle

- Peripheral muscle has a mean CT value of μ = + 44 HU with σ =14 HU; thickness varies from 6 to10 mm.
- Voxels found within 10 mm from the inner boundary of peripheral fat and within the range $44 \pm 2 \times 14$ HU are classified as peripheral muscle.
- The peripheral fat region obtained is dilated using a disk-shaped structuring element of radius 2 mm to remove discontinuities and holes between the peripheral fat and the peripheral muscle.

Preprocessing Steps

Removal of peripheral artifacts and tissues:

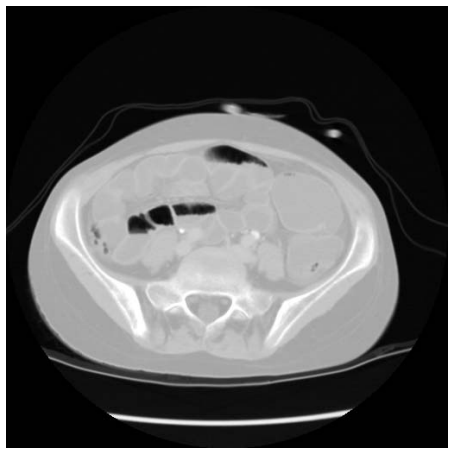

before processing

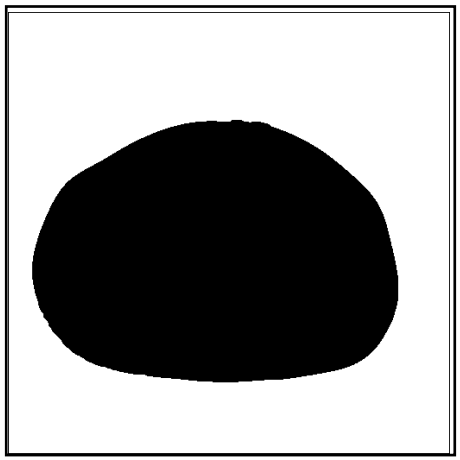

peripheral artifacts

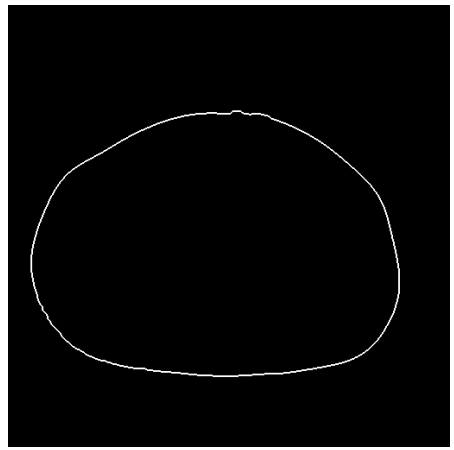

the skin layer

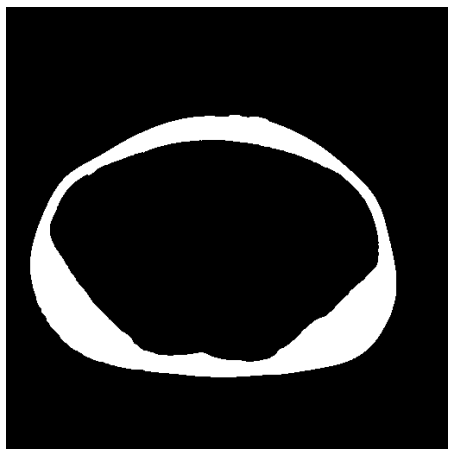

the peripheral fat region

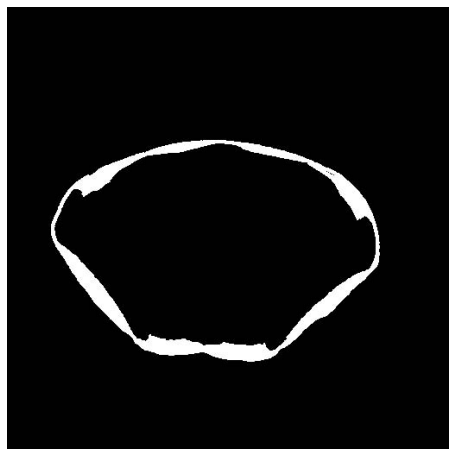

the peripheral muscle

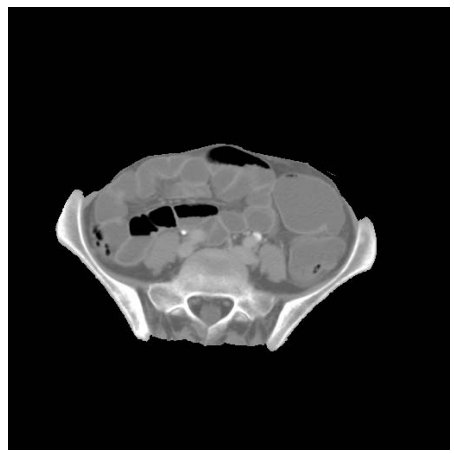

after processing

Preprocessing Steps

Surface after removal of:

peripheral artifacts | the skin layer | the peripheral fat | the peripheral muscle

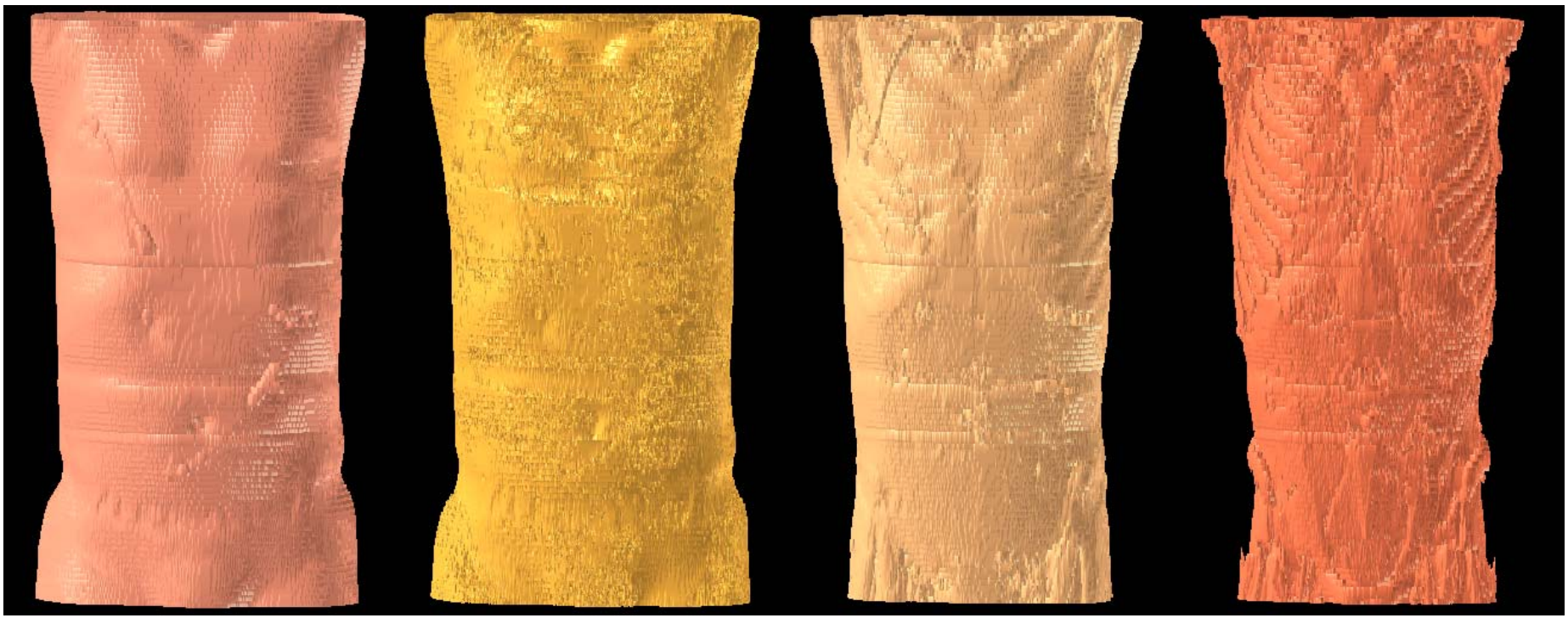

Segmentation of the Rib Structure

Initial segmentation performed using

- thresholding at 200 HU,
- morphological erosion and closing,
- information related to the peripheral fat boundary,
- several features of each thresholded region on each slice:

  - Euclidean distances,
  - compactness $cf = 1 - 4\pi A/P^2$,
  - length and width of each region.

Segmentation of the Rib Structure

- Initial result of segmentation used as a marker to perform opening-by-reconstruction.
- Refined using the features defined previously, defined central line, and an elliptical region obtained adaptively inside the ribs on each slice.

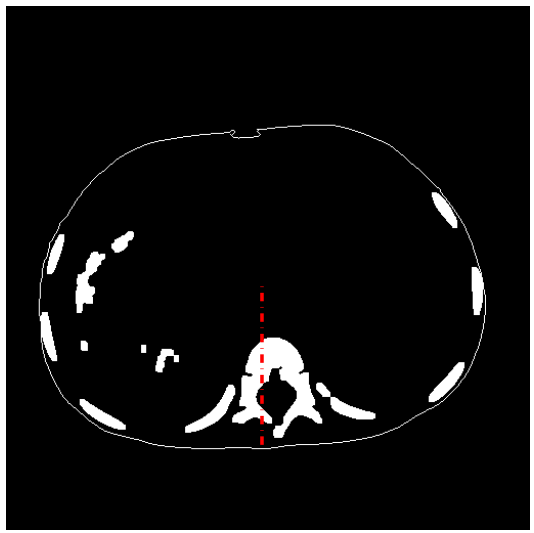

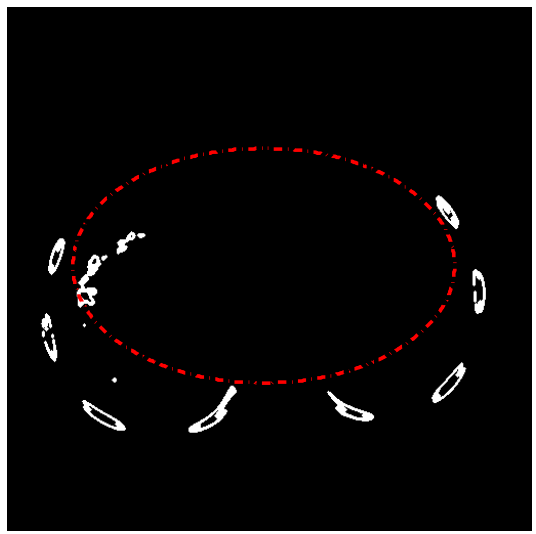

Results: Rib Structure

Produced good results without including parts of tumors or other organs.

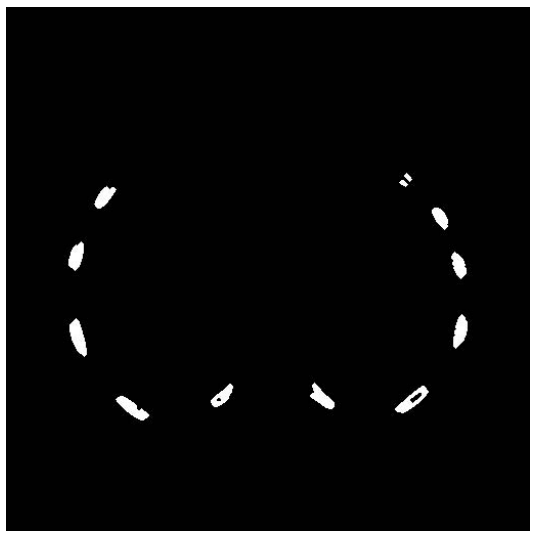

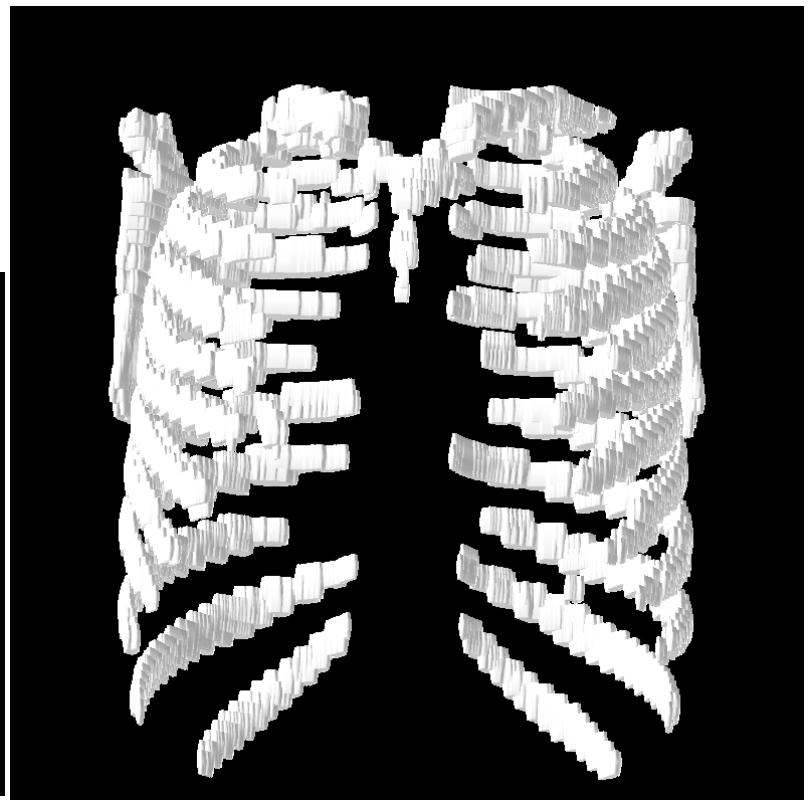

Segmentation of the Vertebral Column

Segmentation performed using:

- the information related to the ribs and the inner boundary of the peripheral fat region,
- thresholding at 180 HU,
- the gradient magnitude, and
- morphological erosion, dilation, and closing.

Segmentation of the Vertebral Column

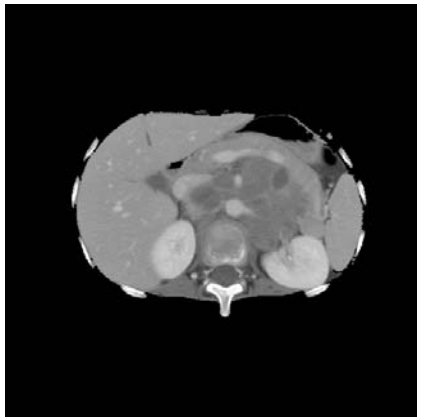

A pre-processed CT slice

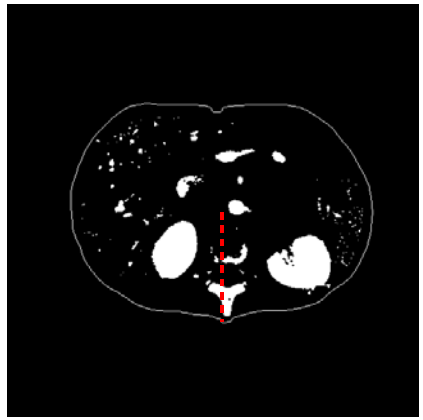

After thresholding and removing the ribs

Initial result of segmentation

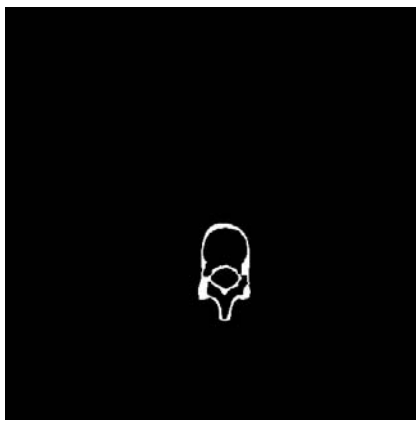

Binarized gradient of the detected region

Region obtained applying the combined mask

Final result of segmentation

Results: Vertebral Column

The results of segmentation compared to manual segmentation performed by a radiologist.

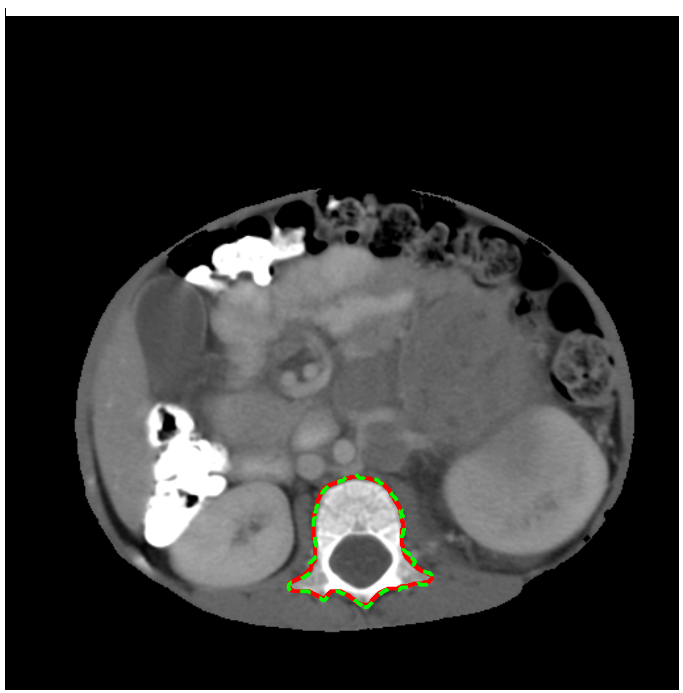

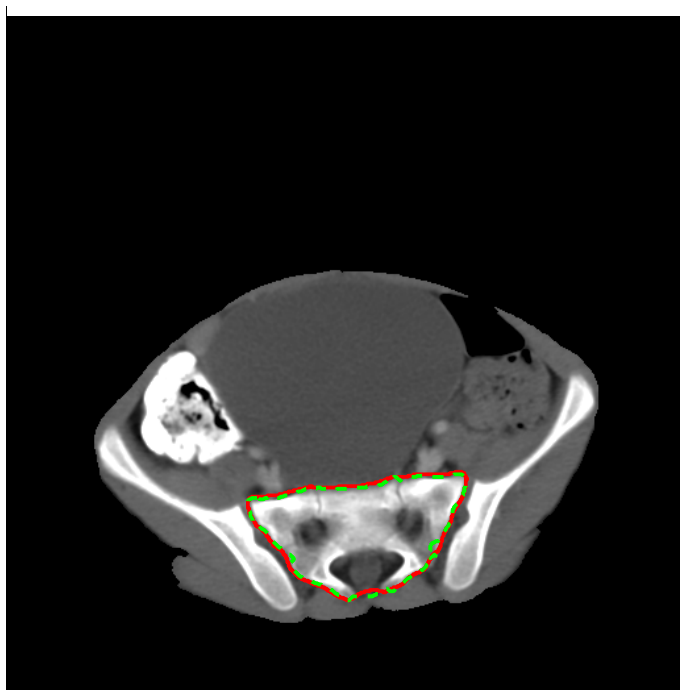

--- *contours drawn by a radiologist*

--- *contours obtained by the proposed methods*

Results: Vertebral Column

Quantitative assessment:

- Number of CT exams: 13 (of 6 patients)
- Number of selected slices: 458
- Average MDCP: 0.73 mm
- Average Hausdorff distance: 3.17 mm

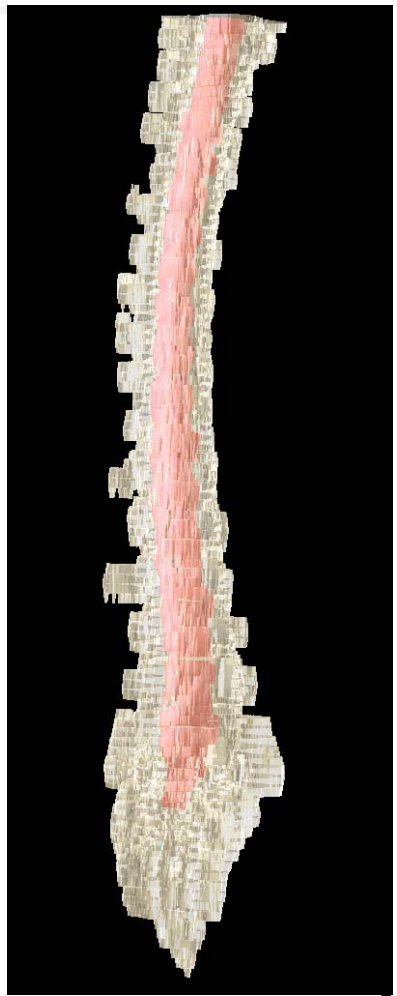

Segmentation of the Spinal Canal

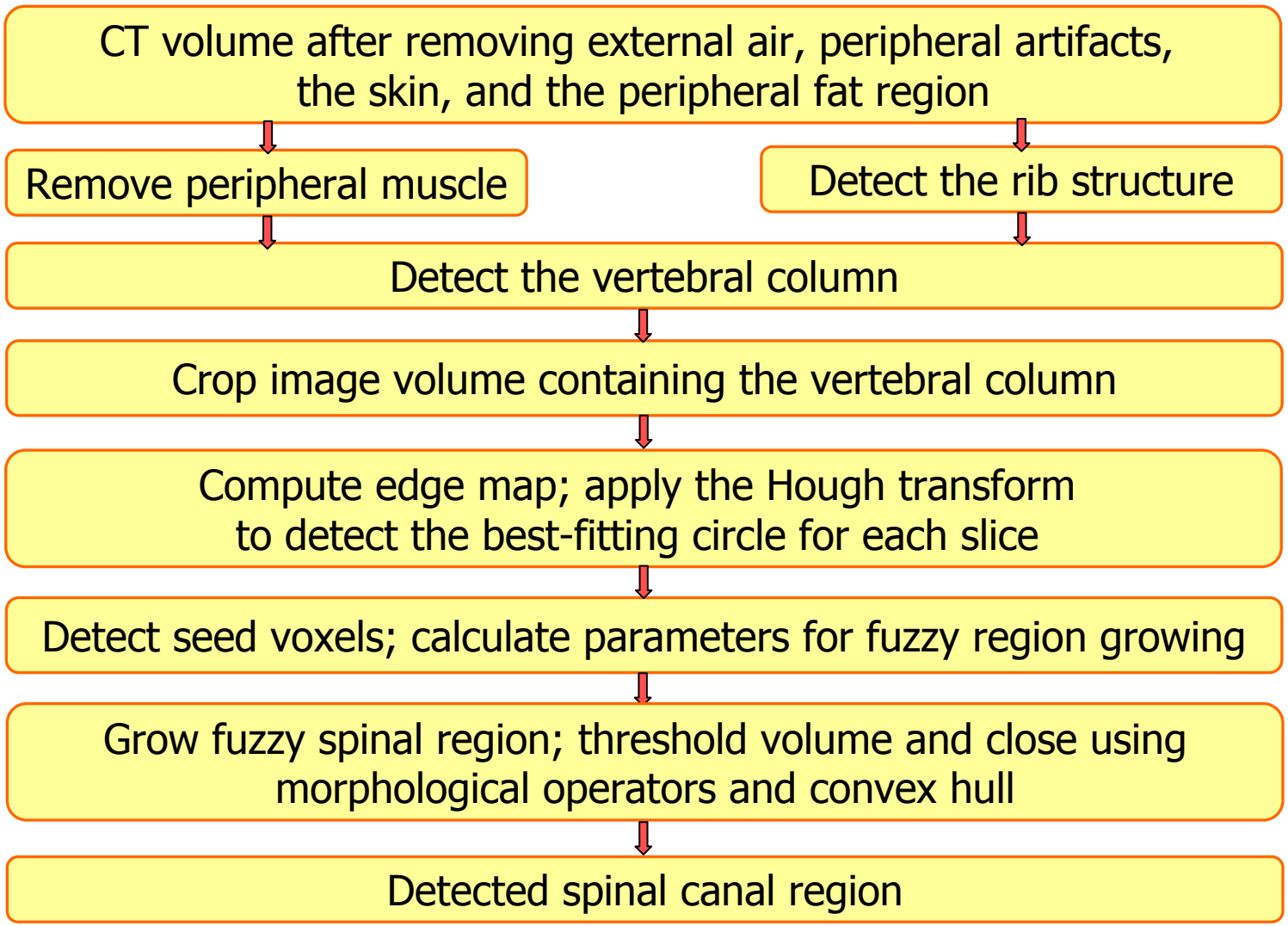

Spinal Canal: Detection of Seed Voxels

- The Hough transform was used to detect the best-fitting circle in the spinal canal.
- The radius of the circle was limited to 6 to 10 mm.
- The vertebral column and the rib structure were used to delimit the search range for seed voxels.
- The center of the detected best-fitting circle with HU values in the range $23 \pm 2 \times 15$ considered as a seed.

Spinal Canal: Detection of Seed Voxels

Original image

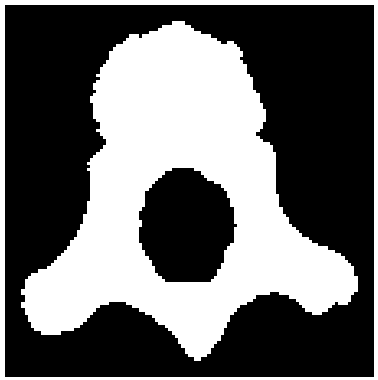

Cropped V.C.

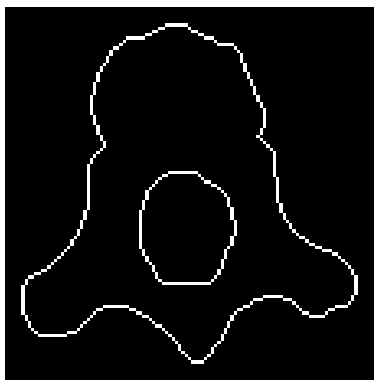

Edge map

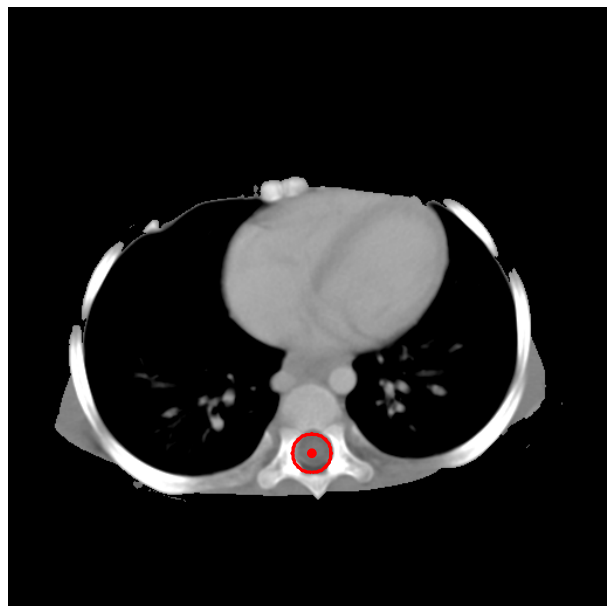

Detected best-fitting circle and its center

V.C.: vertebral column

Spinal Canal: Detection of Seed Voxels

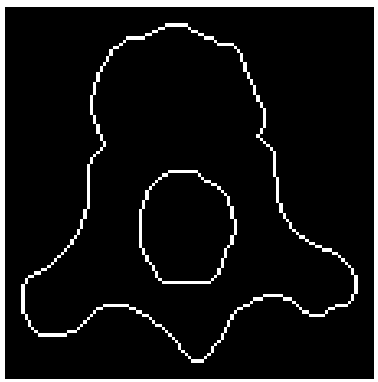

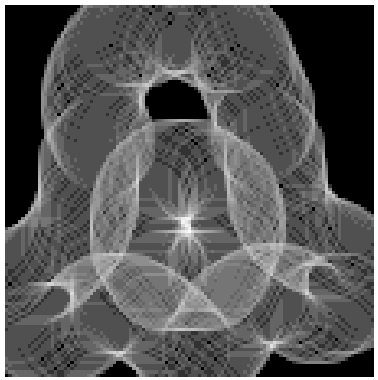

c=15 pixels
=6.15 mm

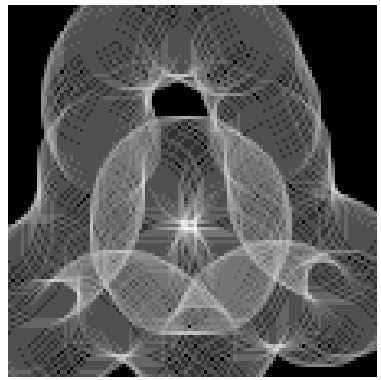

c=16 pixels
=6.56 mm

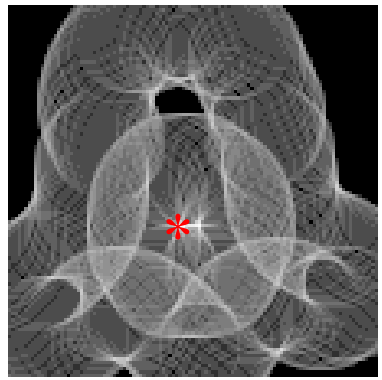

c=17 pixels
=6.97 mm

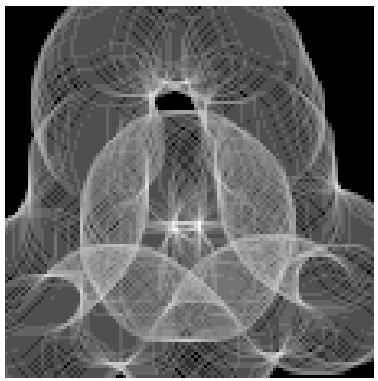

c=18 pixels
=7.38 mm

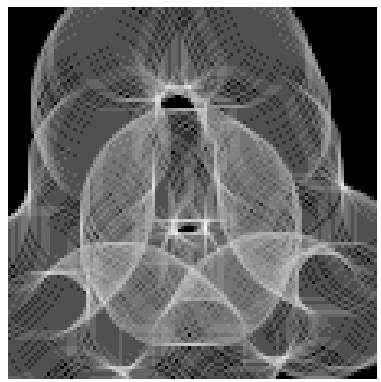

c=19 pixels
=7.79 mm

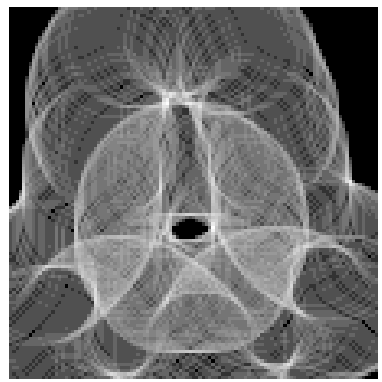

c=21 pixels
=8.61 mm

Spinal Canal: Detection of Seed Voxels

Original image

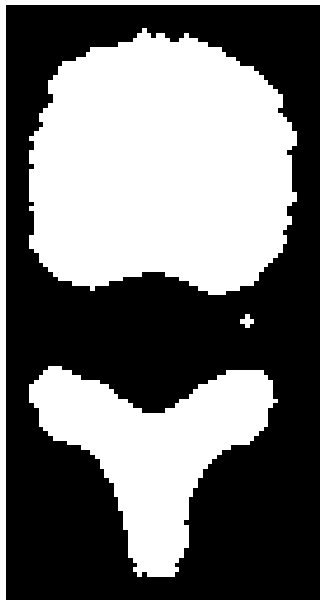

Cropped V.C.

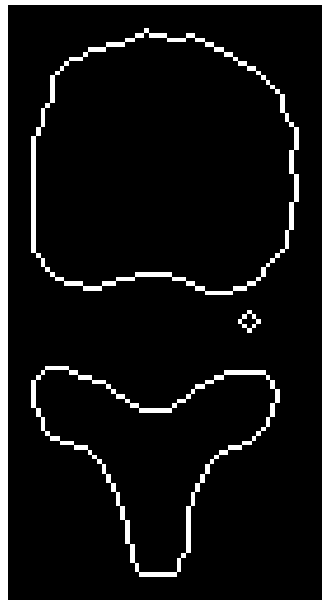

Edge map

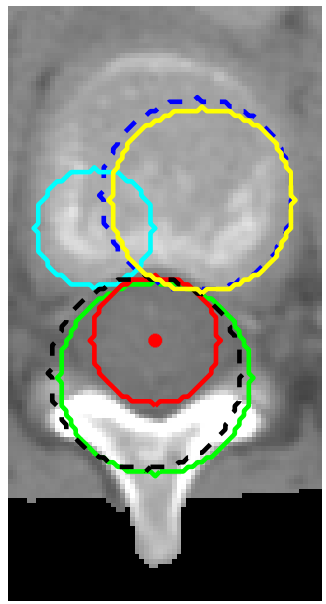

Candidate circles

Spinal Canal: Detection of Seed Voxels

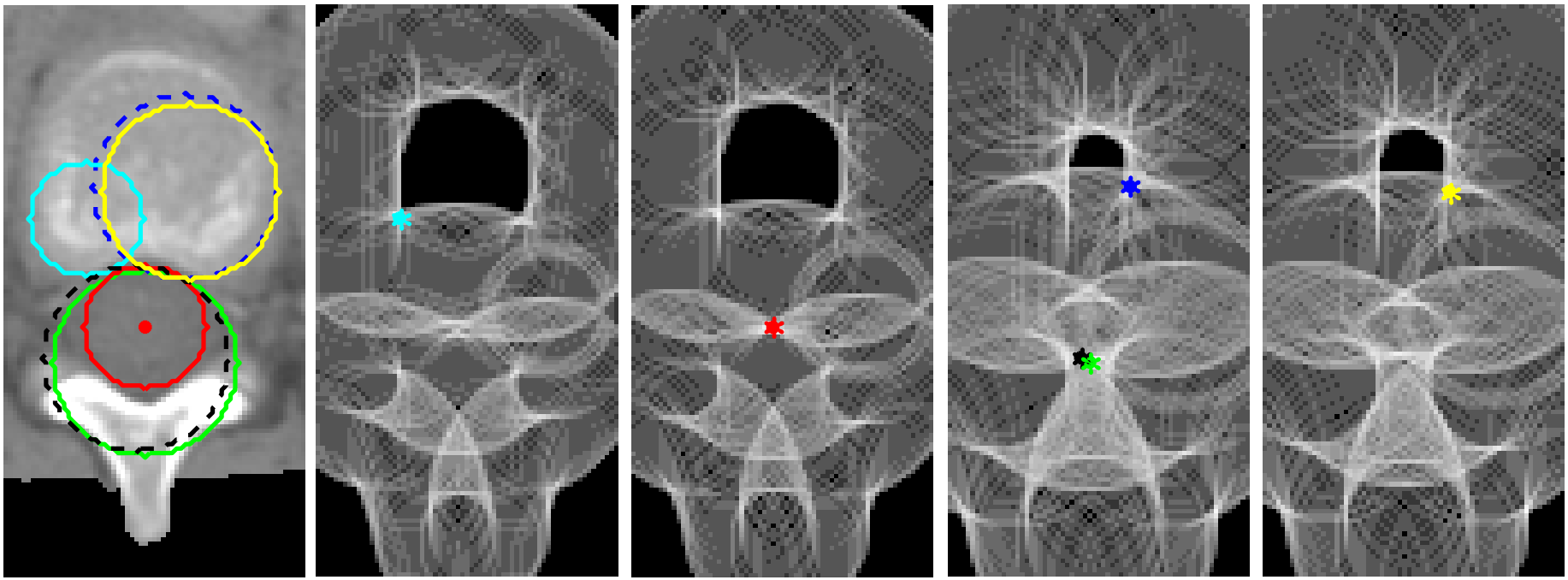

c=13 pixels =7.15 mm

c=14 pixels =7.70 mm

c=20 pixels =11.00 mm

c=21 pixels =11.55 mm

Segmentation of the Spinal Canal

- Segmentation performed using fuzzy mapping and opening-by-reconstruction.
- The detected seed voxels from a number of slices in the thoracic region were used as markers.
- The mean and the standard deviation calculated within the neighborhood of 21 x 21 pixels of each of the seed voxels.
- The result morphologically closed using a tubular structuring element with radius 2 mm and height 10 mm, and the convex hull.

Results: Spinal Canal

--- contours drawn by a radiologist

--- contours obtained by the proposed methods

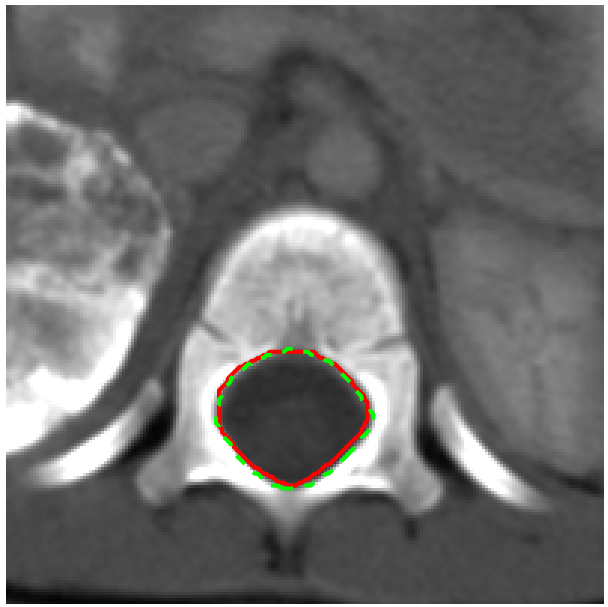

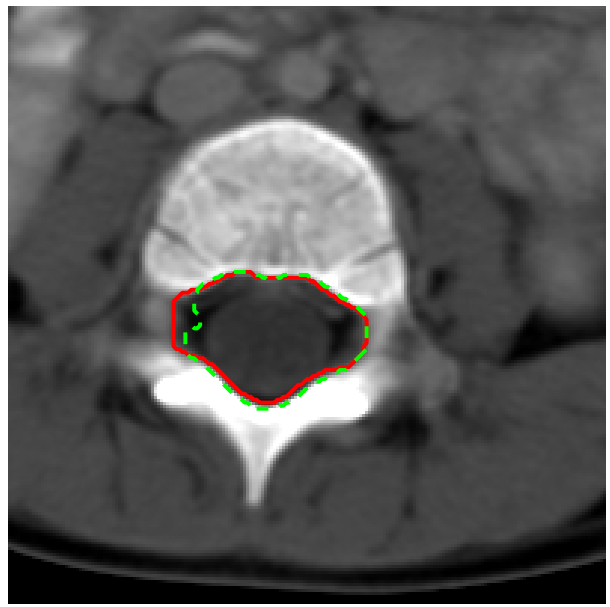

Results: Spinal Canal

Quantitative assessment:

- Number of CT exams: 3
- Number of selected slices: 21
- Average MDCP: 0.62 mm
- Average Hausdorff distance: 1.60 mm

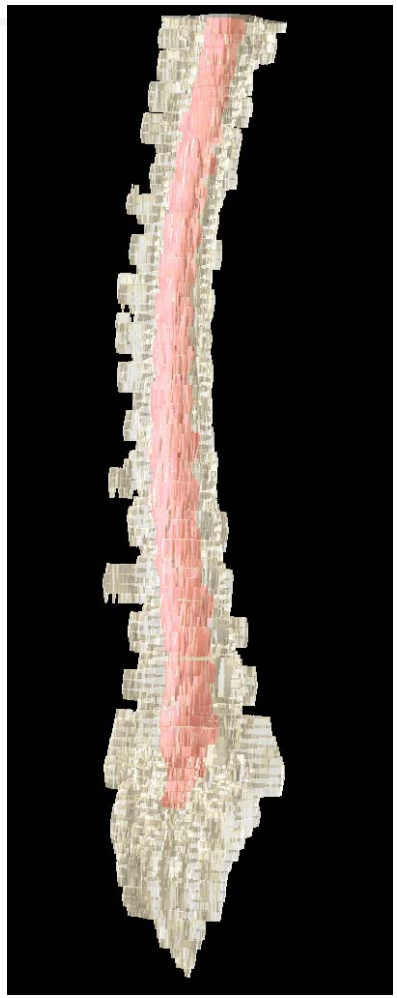

Diaphragm

- Double-domed muscle separating the thorax from the abdomen.
- Directly below the lungs: extract the lower surfaces of the lungs and use them to obtain the diaphragm.
- Model each dome using linear least-squares and obtain final representation using deformable contours.

Delineation of the Diaphragm

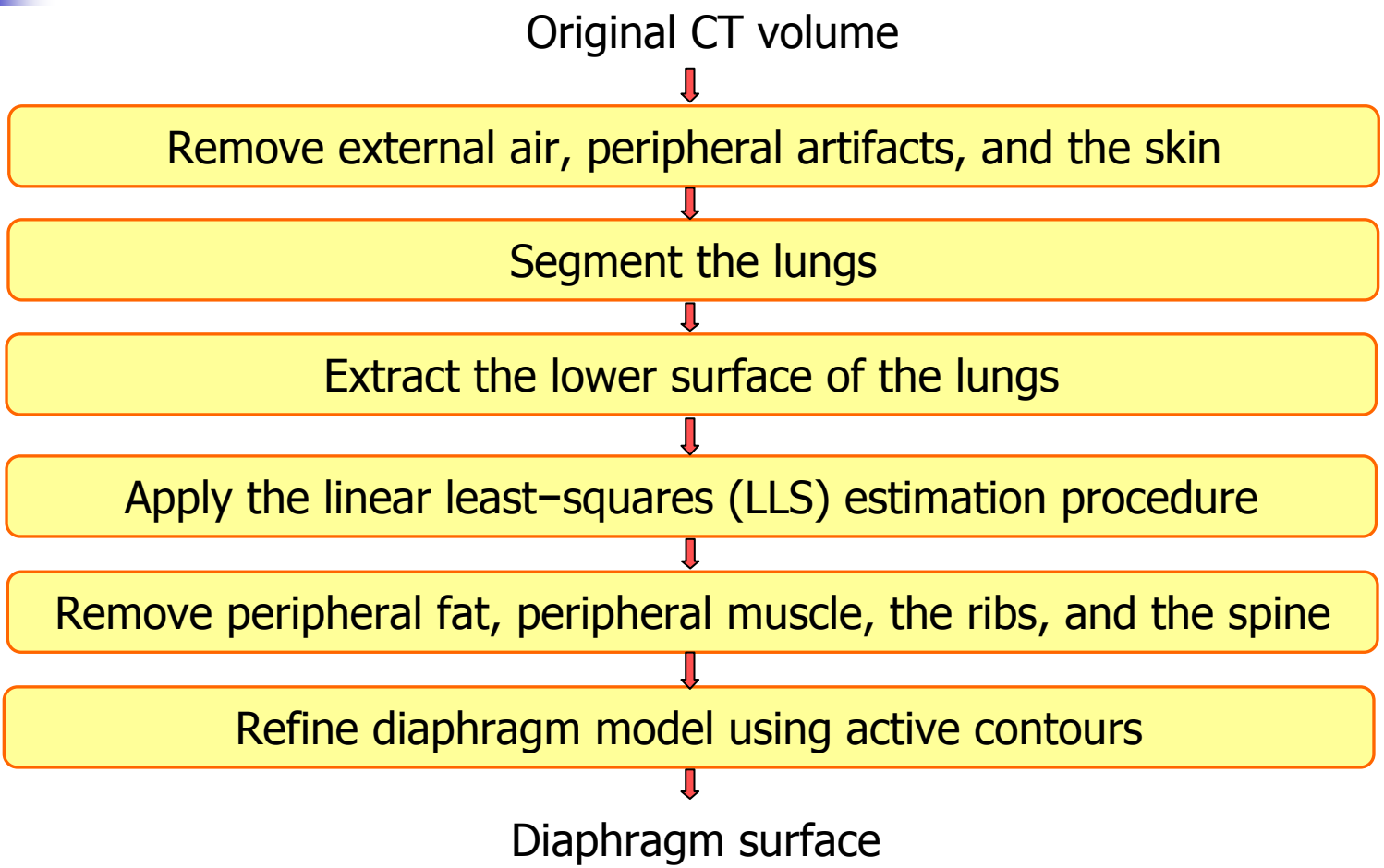

Segmentation of the Lungs

- Easily distinguishable from the rest of body.
- The lungs form the single-largest volume of air in the body.
- Iterative procedure to determine the optimal threshold:

$$T_{i+1} = \frac{\mu_b + \mu_n}{2}, \; i = 1, 2, ...$$

- Procedure modified for children to exclude air regions inside bowels.

Segmentation of the Lungs: Results

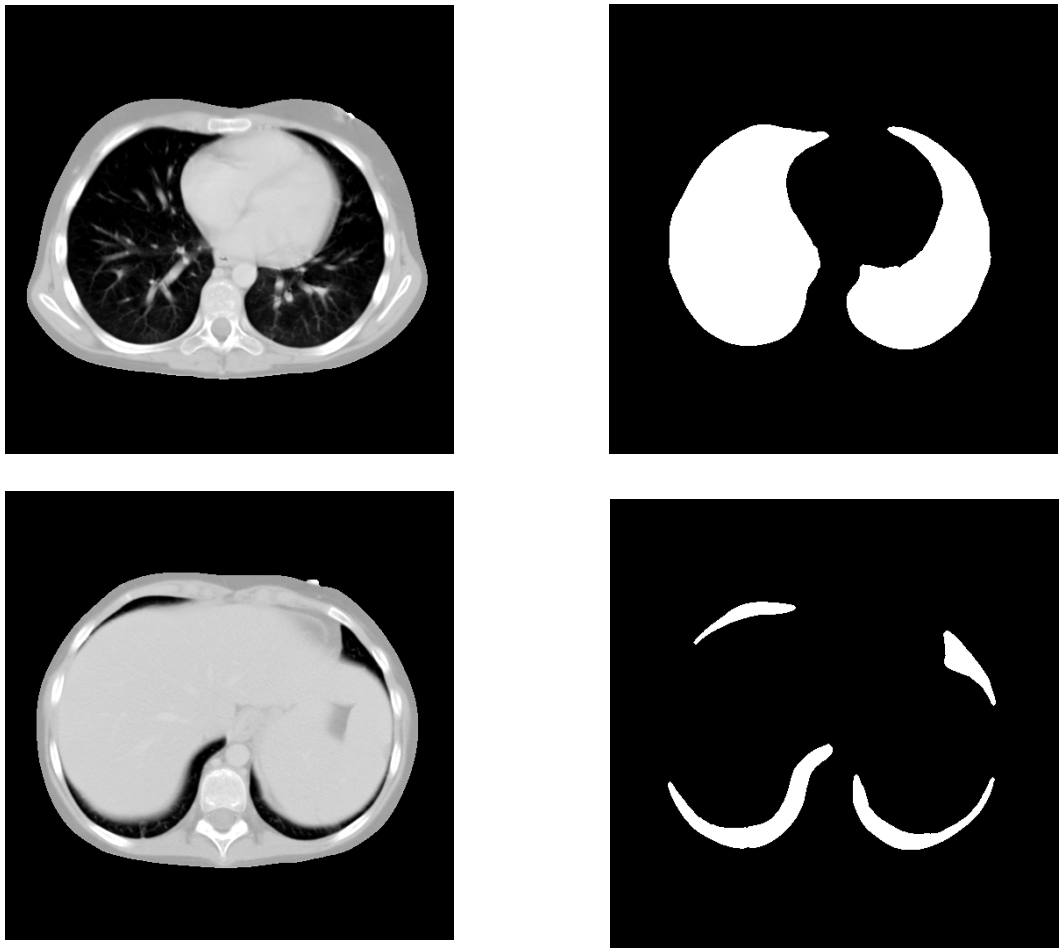

Delineation of the Diaphragm

Representation of the diaphragm using LLS:

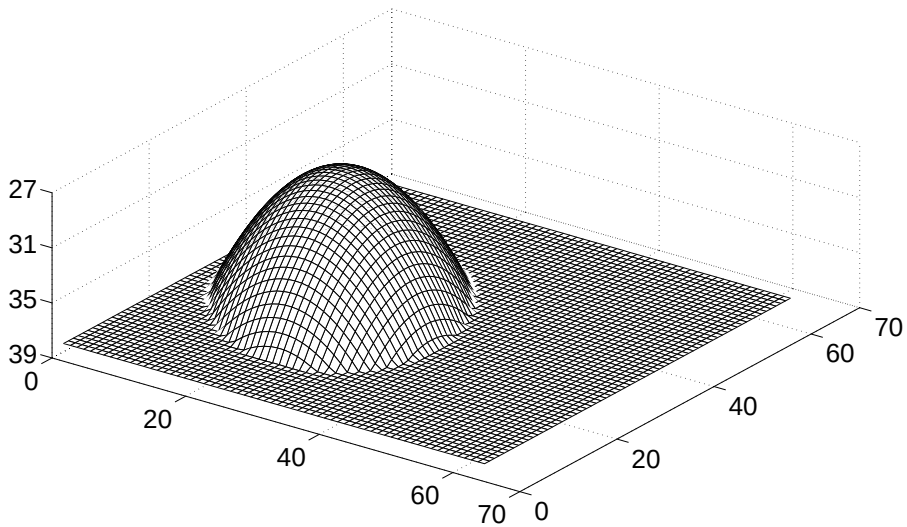

right-dome surface

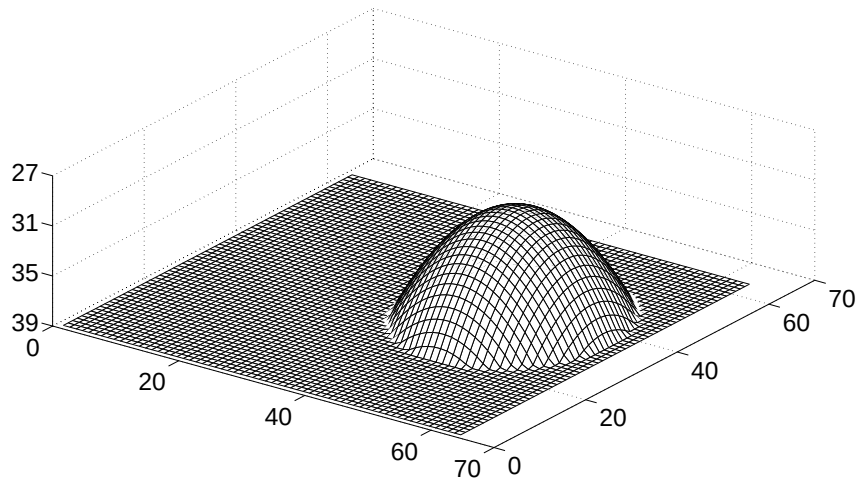

left-dome surface

Delineation of the Diaphragm

Representation of the diaphragm using LLS and active contours:

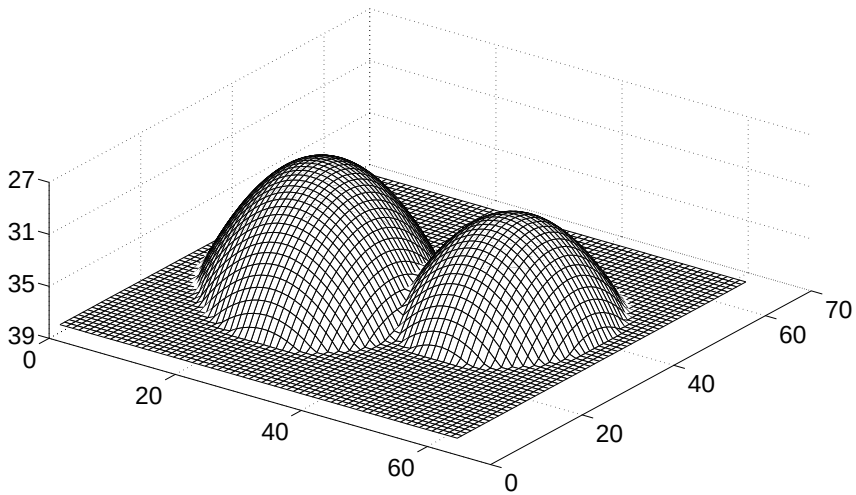

combined surface

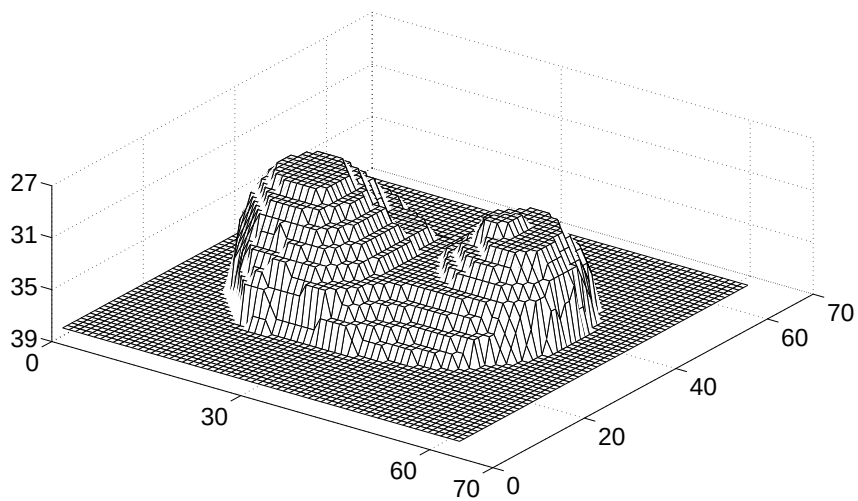

after applying active contour

Delineation of the Diaphragm

Representation of the diaphragm using LLS and active contours:

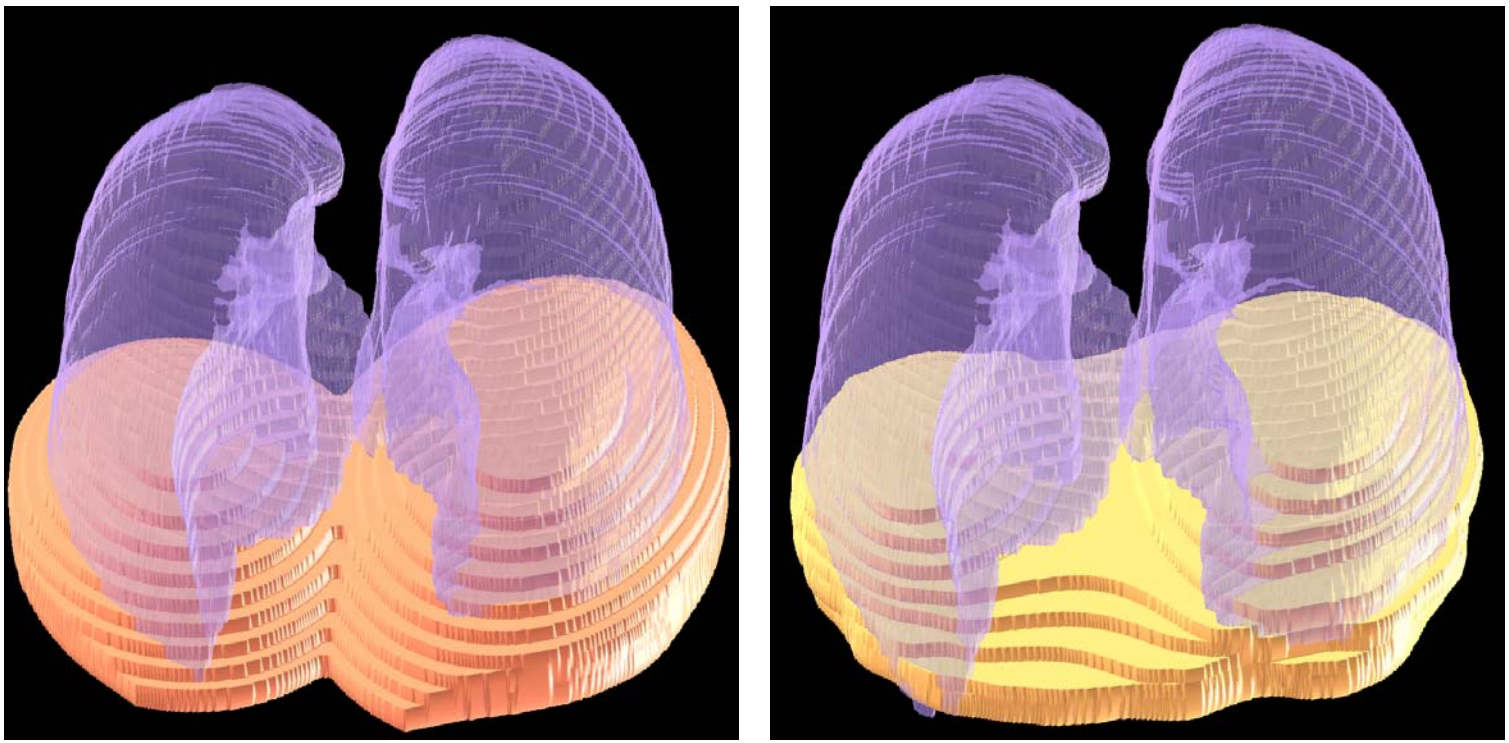

Segmented lungs and the diaphragm

Results: Diaphragm

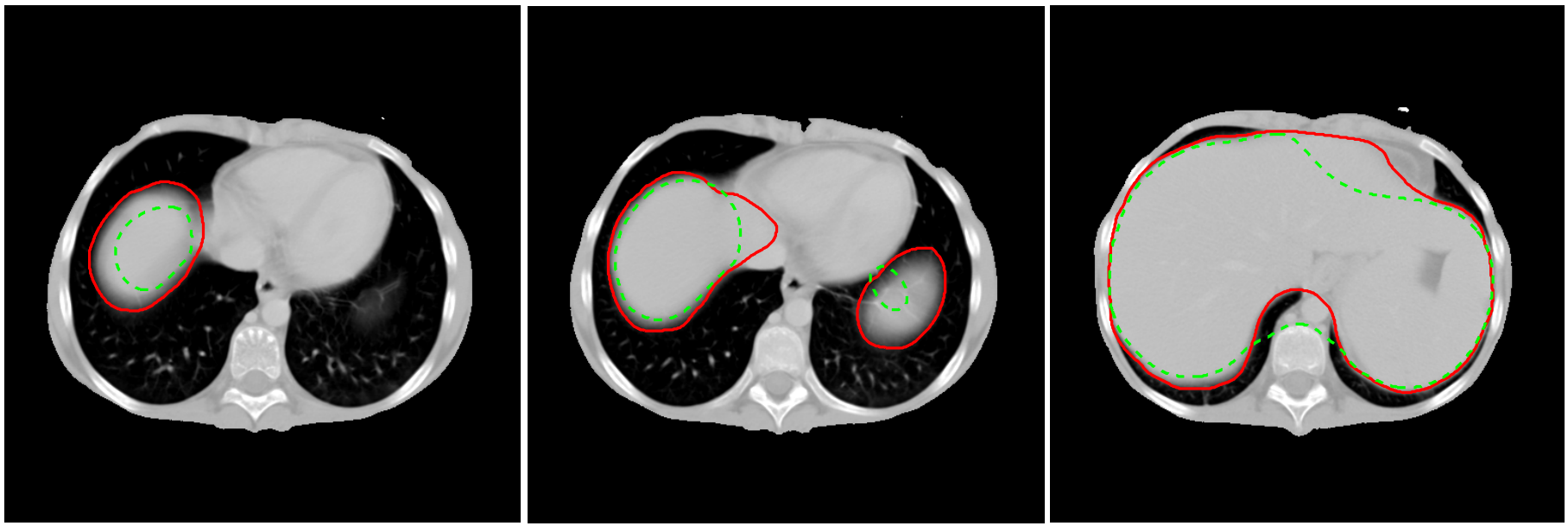

--- *contours drawn by a radiologist*

--- *contours obtained by the proposed methods*

Results: Diaphragm

Quantitative assessment:

- Number of CT exams: 11 (of six patients)
- Number of selected slices: 109
- Average MDCP in 3D: 6.05 mm
- Average maximum Hausdorff distance in 3D: 28.03 mm

Removal of the Thoracic Cavity

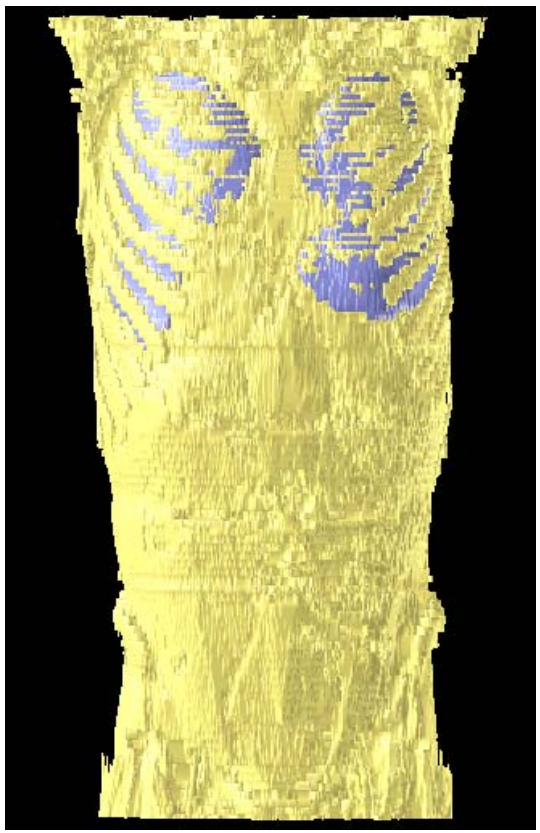

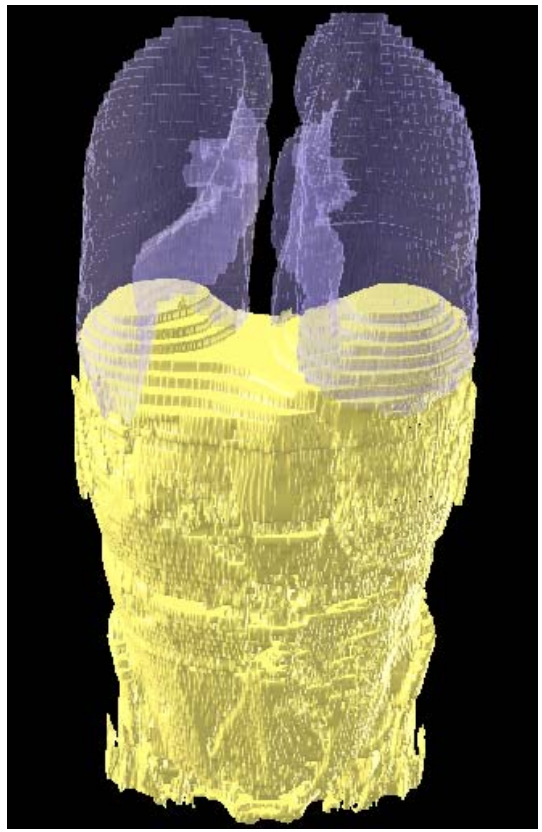

Delineation of the Pelvic Girdle

Automatic detection of seed voxels using information related to

- the spinal canal,
- the vertebral column, and
- the peripheral fat boundary.

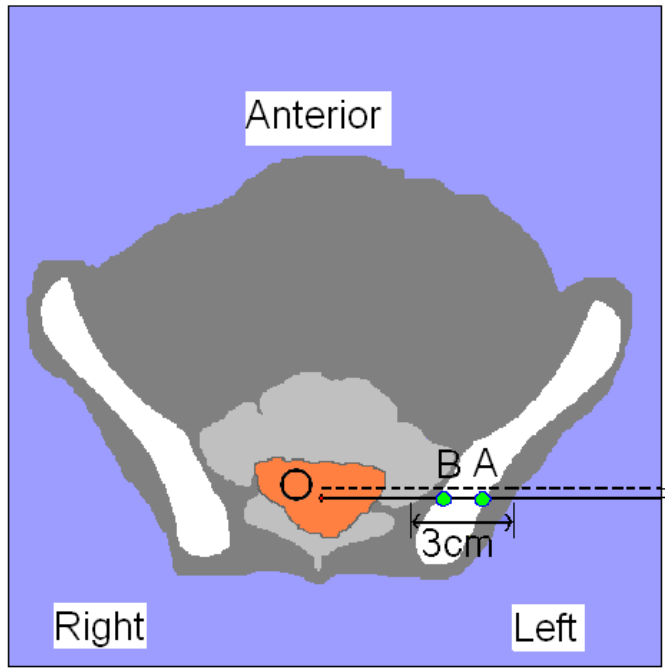

Delineation of the Pelvic Girdle

Automatic segmentation performed using fuzzy mapping and opening-by-reconstruction (in 3D).

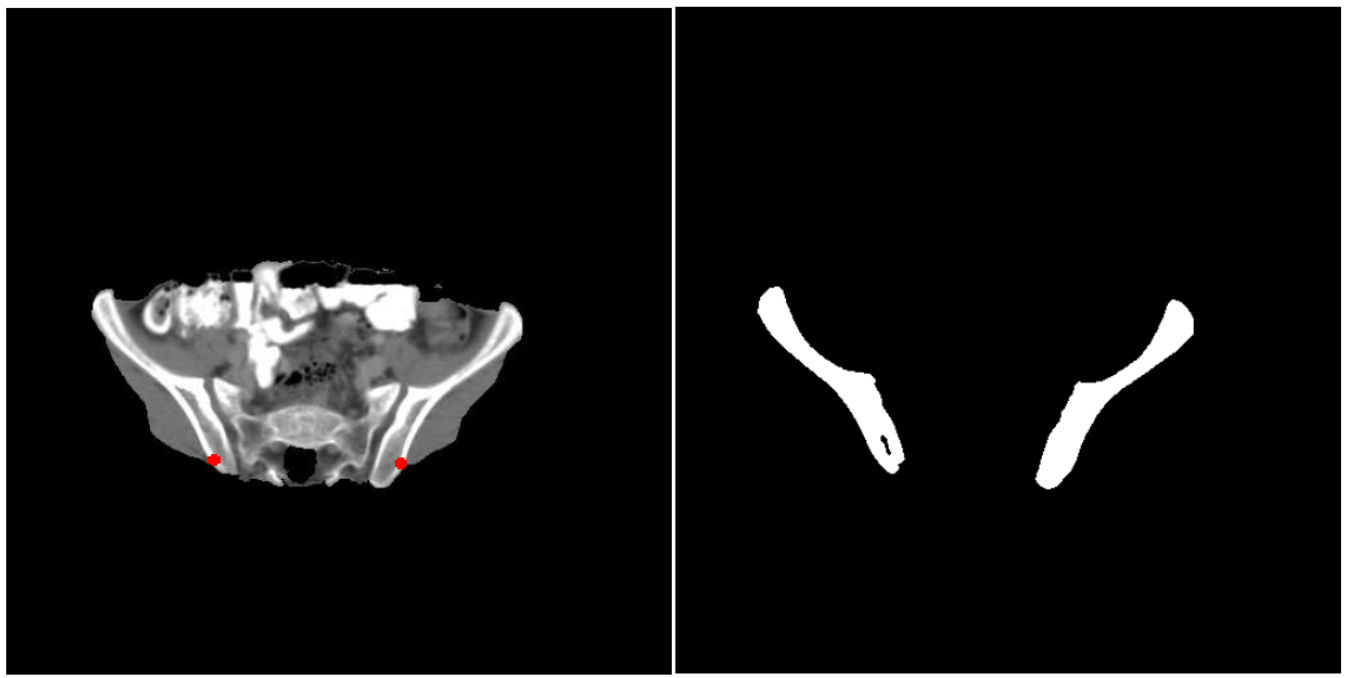

Results: Pelvic Girdle

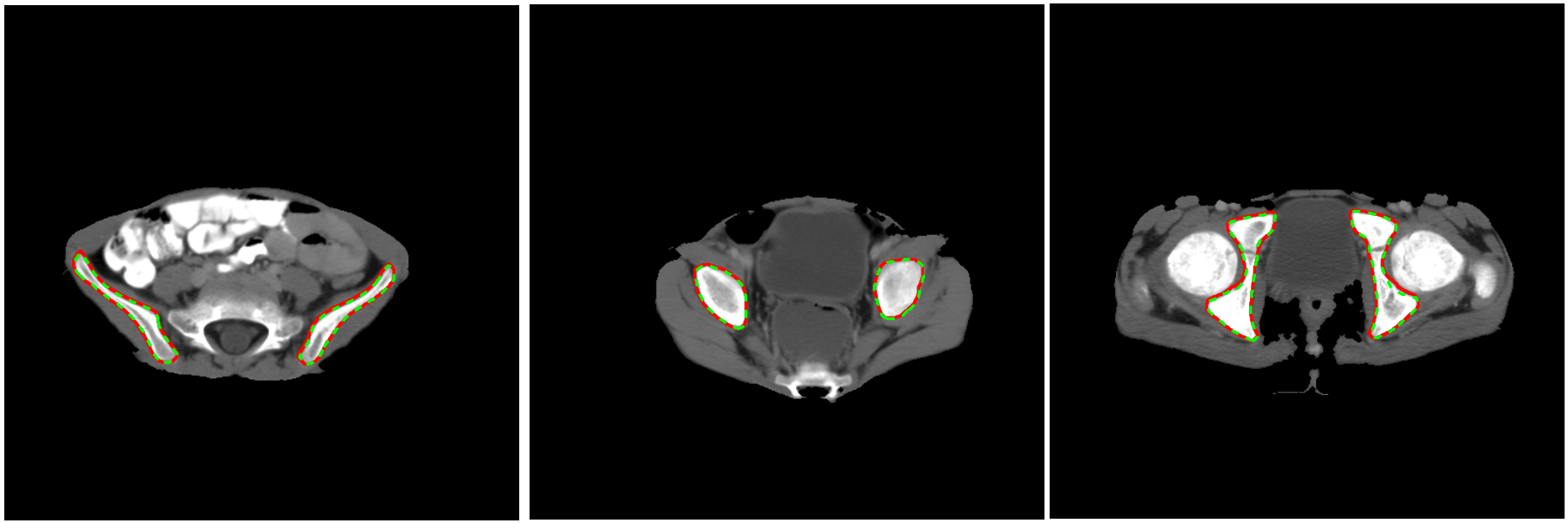

contours drawn by a radiologist

contours obtained by the proposed methods

Results: Pelvic Girdle

Quantitative assessment:

- Number of CT exams: 13 (of six patients)
- Number of selected slices: 277
- Average MDCP in 3D: 0.53 mm
- Average maximum Hausdorff distance in 3D: 5.95 mm

Modeling the Upper Surface of the Pelvic Girdle

Representation of the upper surface of the pelvic girdle using the LLS model and active contours:

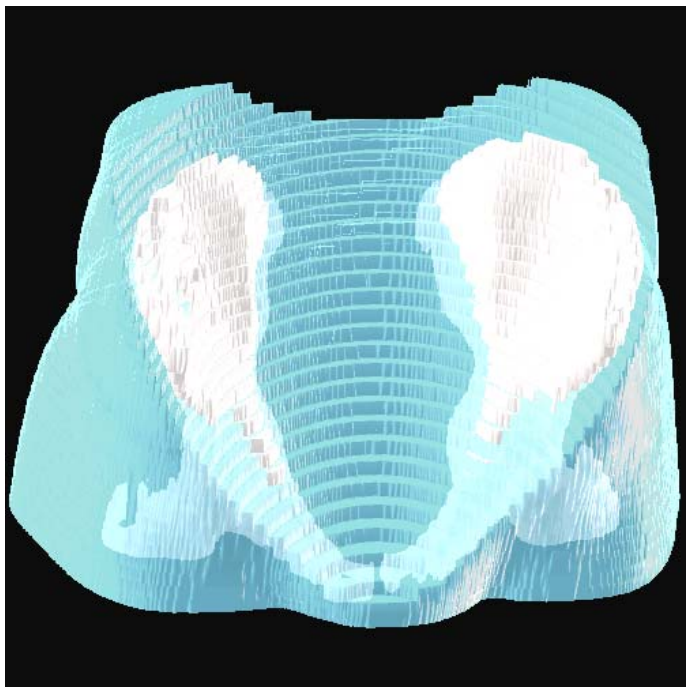

Linear least-squares model

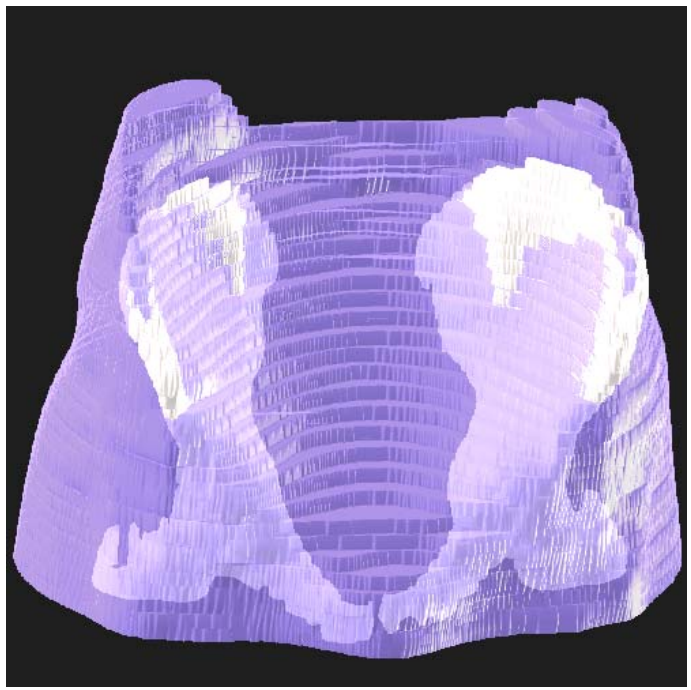

Refined pelvic surface

Removal of the Pelvic Cavity

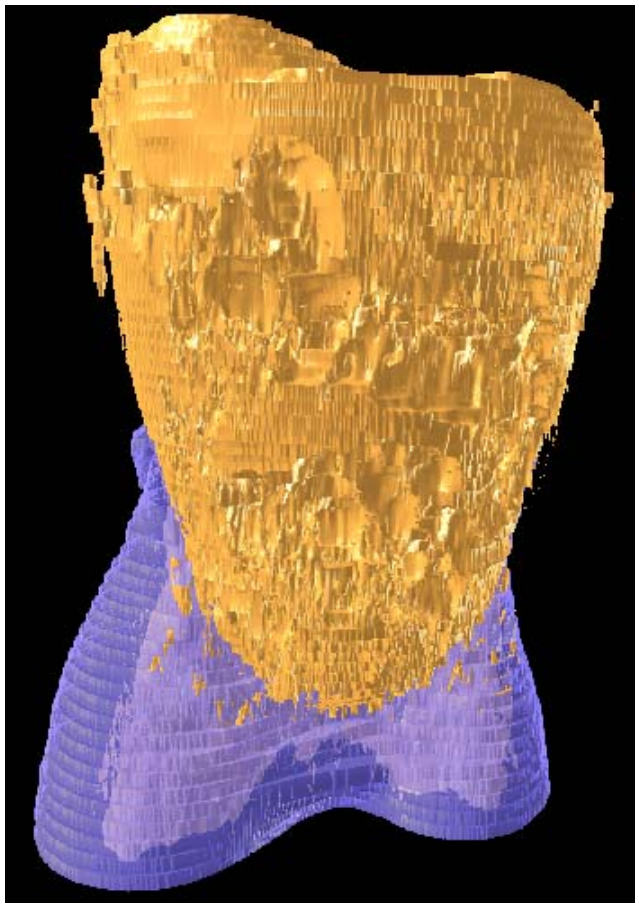

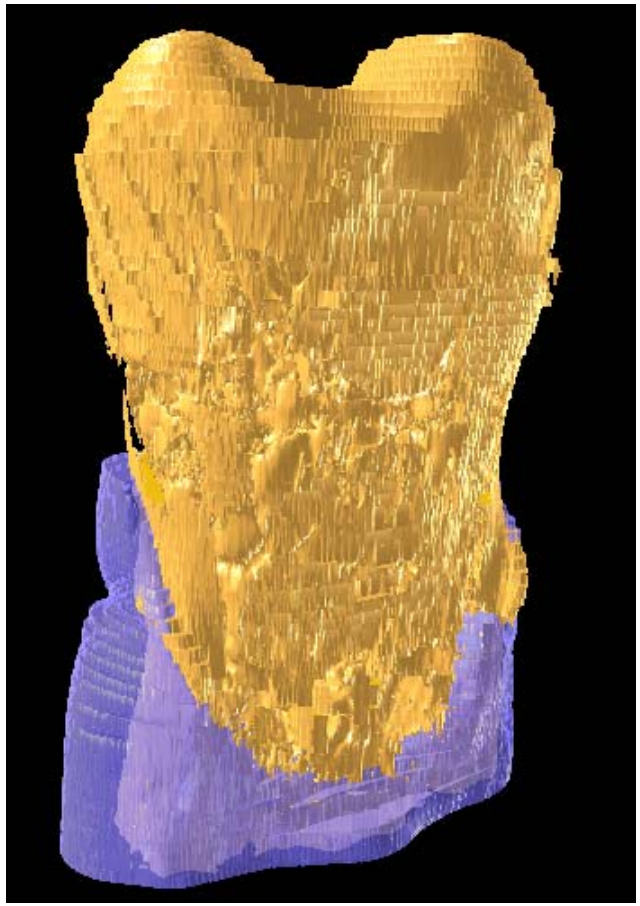

Results: Landmarks Identified

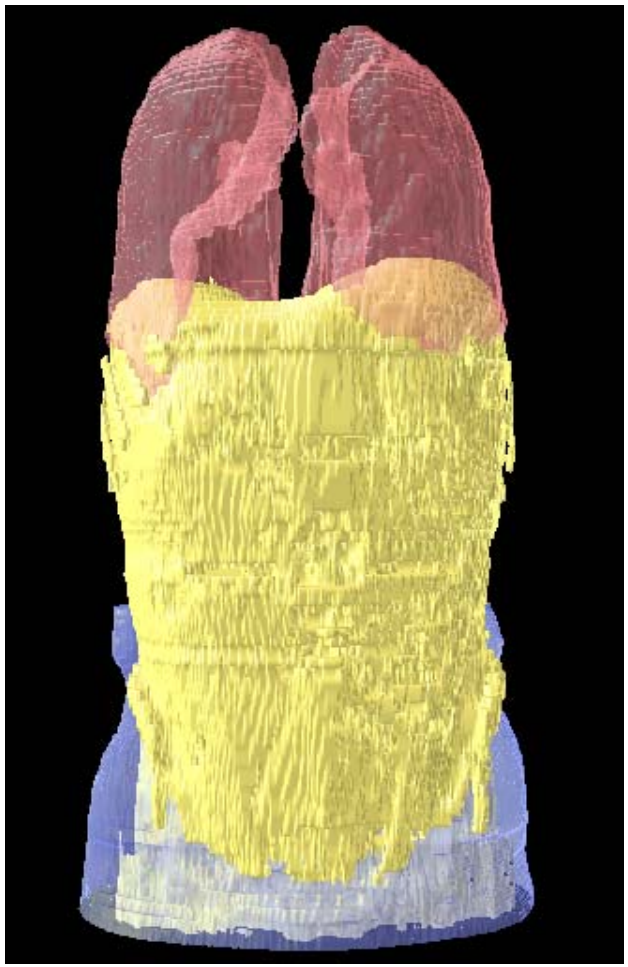

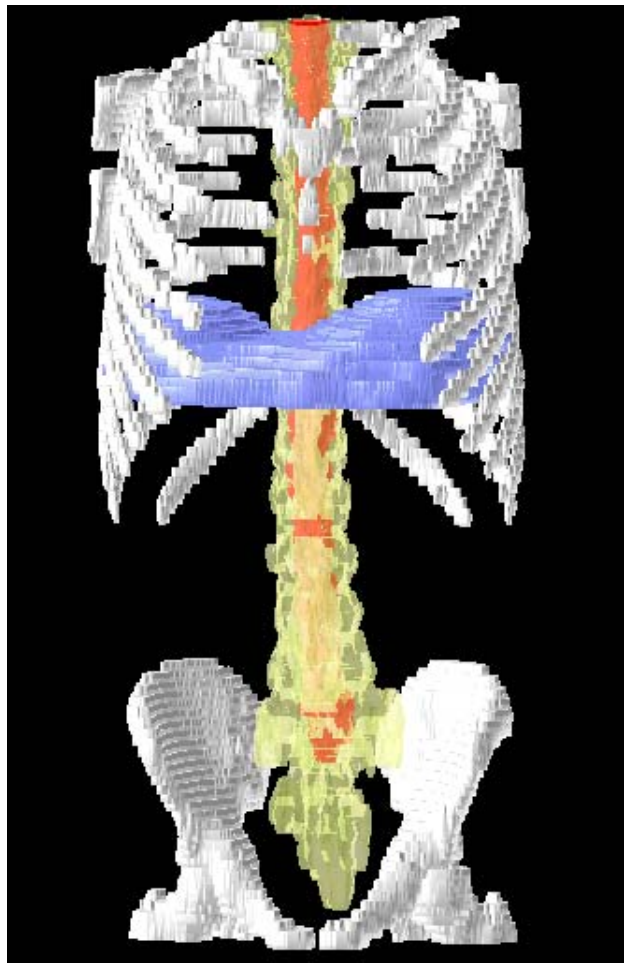

Application to the Segmentation of Neuroblastic Tumors

Neuroblastoma

- Malignant tumor
- Originates along the sympathetic ganglia or in the adrenal medulla.
- Accounts for **8—10%** of all childhood cancers.
- **65%** of the tumors are located in the abdomen.

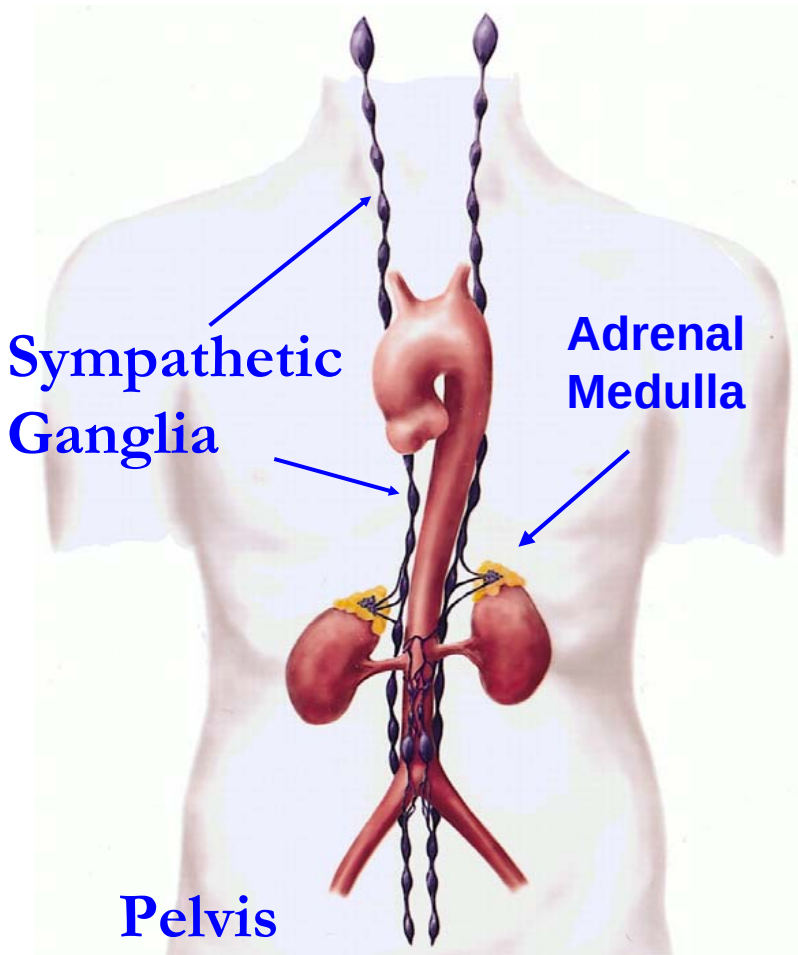

CT Image of Neuroblastoma

- Abdominal tumors are most common: the worst prognosis.

- Generally heterogeneous, with a mixture of:

  - necrosis (low density),
  - viable tumor (medium density),
  - calcification (high density).

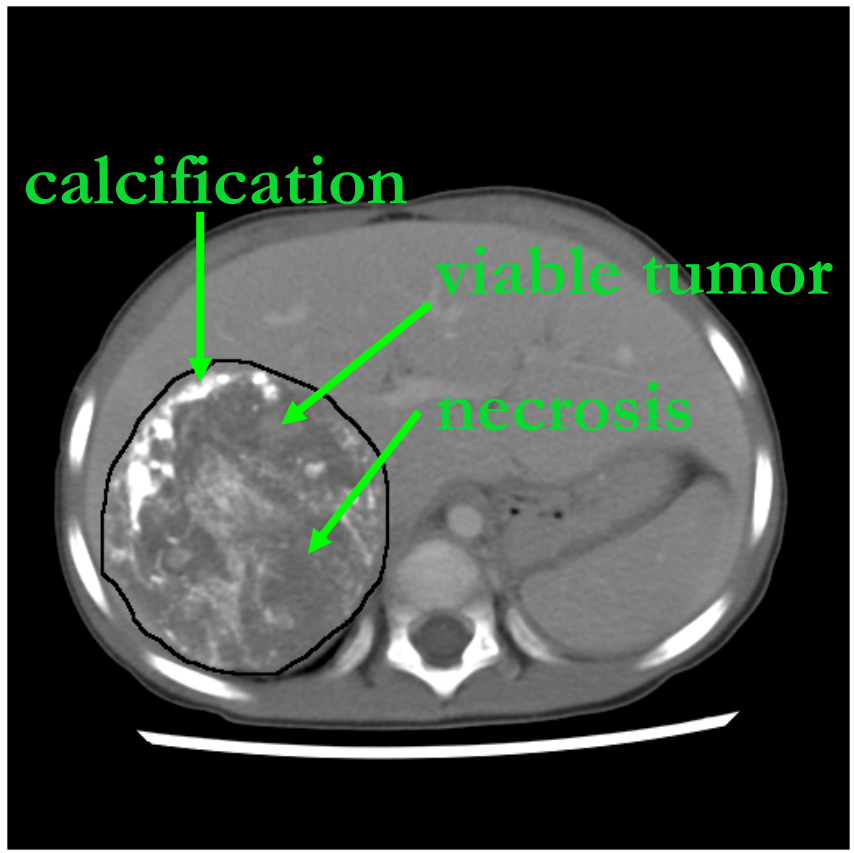

Tumor Response to Therapy

- Tumor shrinks

  Intermediate density: active or viable tumor

  → Low density: necrosis

  → High density: calcified tissue

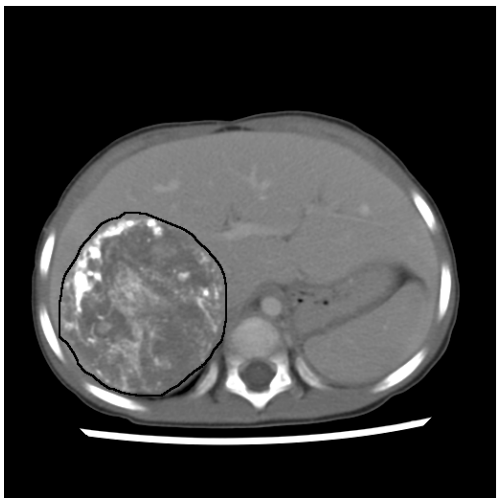

April 2001

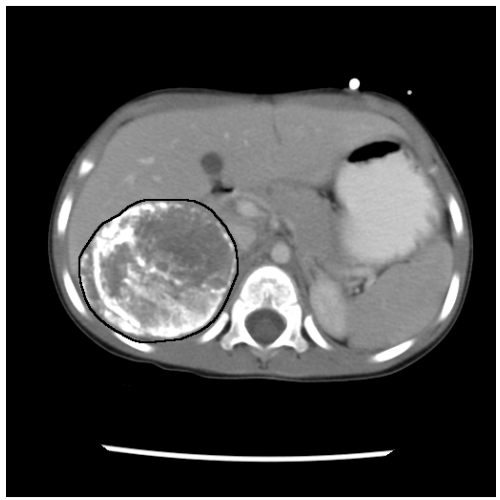

June 2001

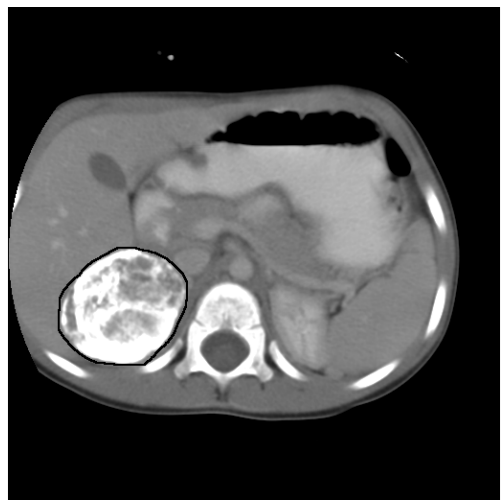

September 2001

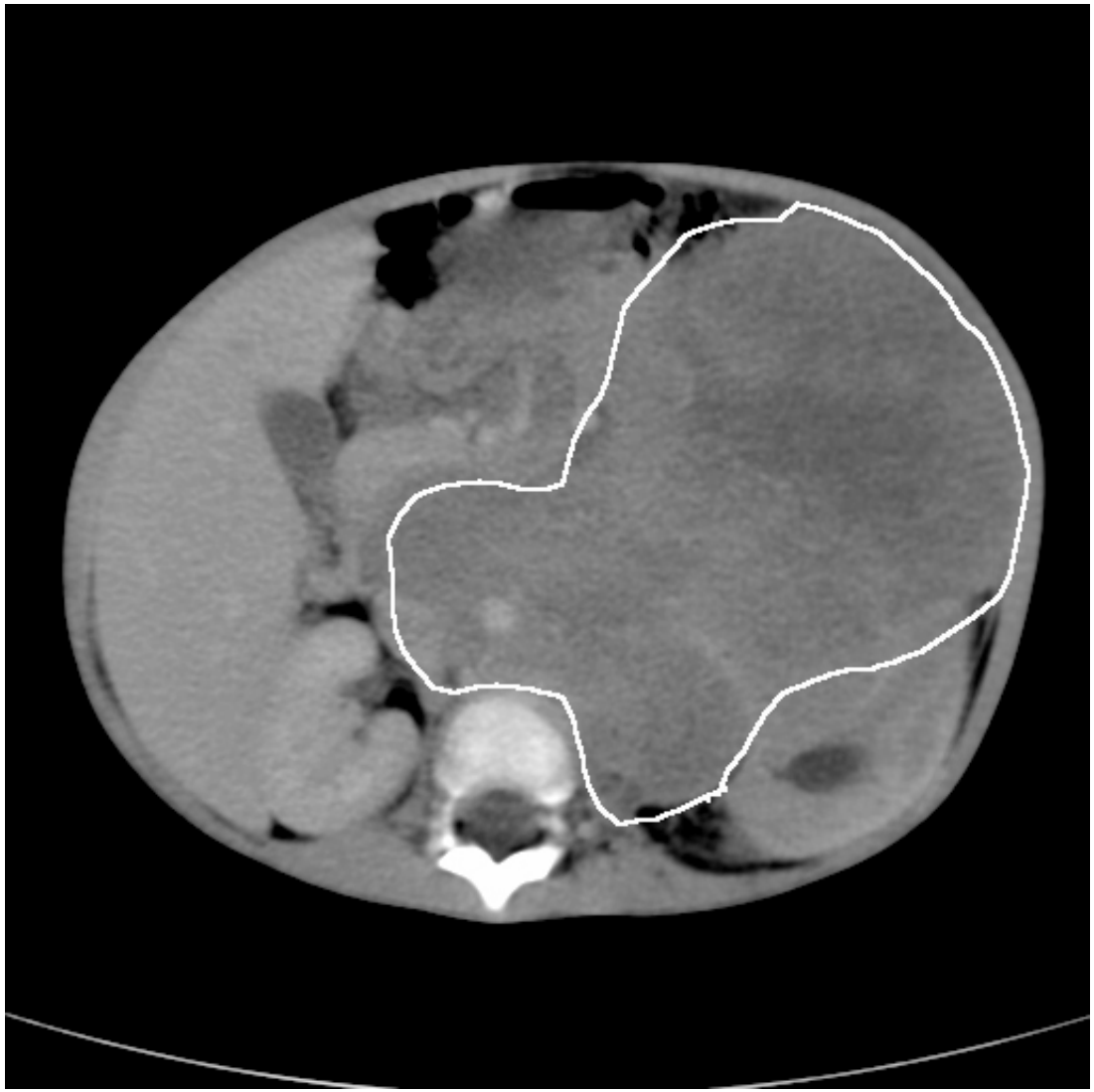

Tumor mass enclosing the aorta: unresectable

Clinical and Image-based Analysis

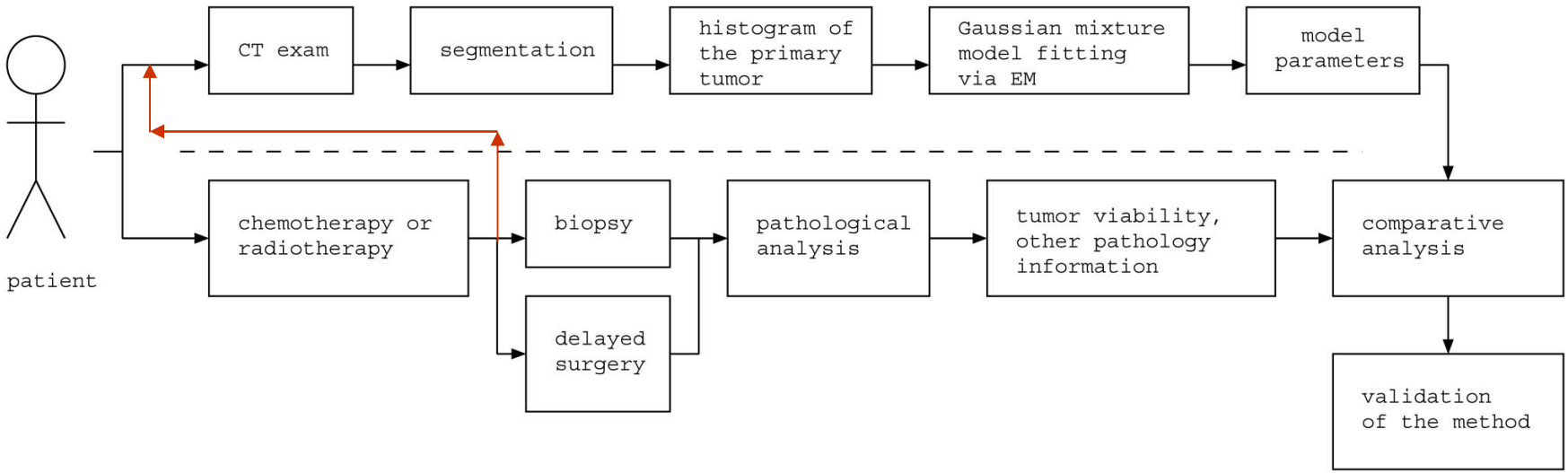

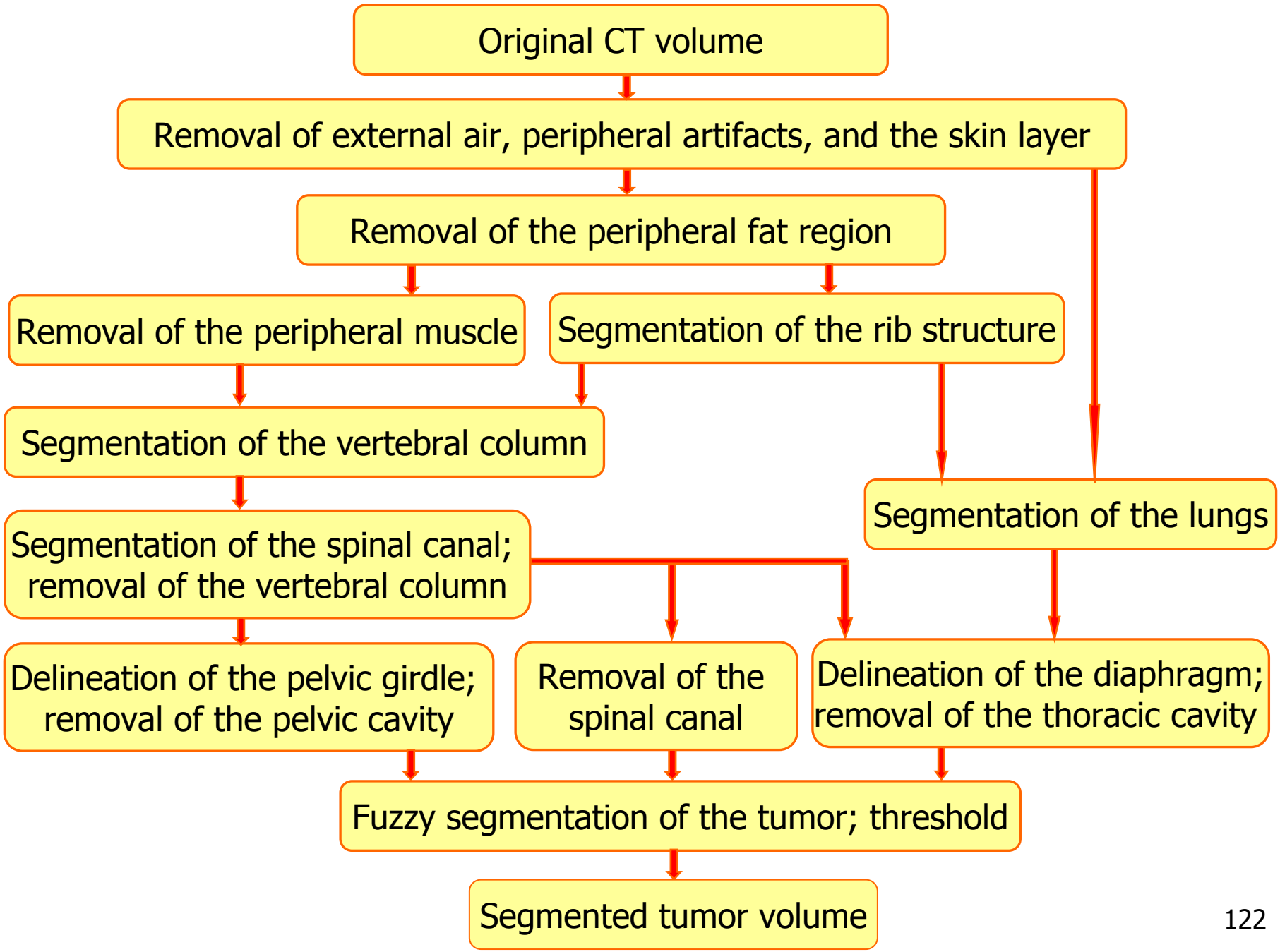
Original CT volume
Removal of external air, peripheral artifacts, and the skin layer
Removal of the peripheral fat region
Removal of the peripheral muscle
Segmentation of the rib structure
Segmentation of the vertebral column
Segmentation of the lungs
Segmentation of the spinal canal; removal of the vertebral column
Delineation of the pelvic girdle; removal of the pelvic cavity
Removal of the spinal canal
Delineation of the diaphragm; removal of the thoracic cavity
Fuzzy segmentation of the tumor; threshold
Segmented tumor volume

Segmentation of the Tumor

1. A region within the tumor mass manually selected.

2. Region statistics, μ_R and σ_R, calculated.

3. Data volume mapped using fuzzy mapping function

$$f_M(r) = \exp\left\{-\frac{1}{2}\left(\frac{r-\mu_R}{\sigma_R}\right)^2\right\}$$

where r is an arbitrary pixel in the image.

Segmentation of the Tumor

4. The selected region is used as a region marker

5. Reconstruction performed to obtain graded connected components using fuzzy-mapped image as mask and the region marker

6. Image thresholded using $T = \mu_R + 0.5\,\sigma_R$

Segmentation of Neuroblastoma: Homogeneous Tumor

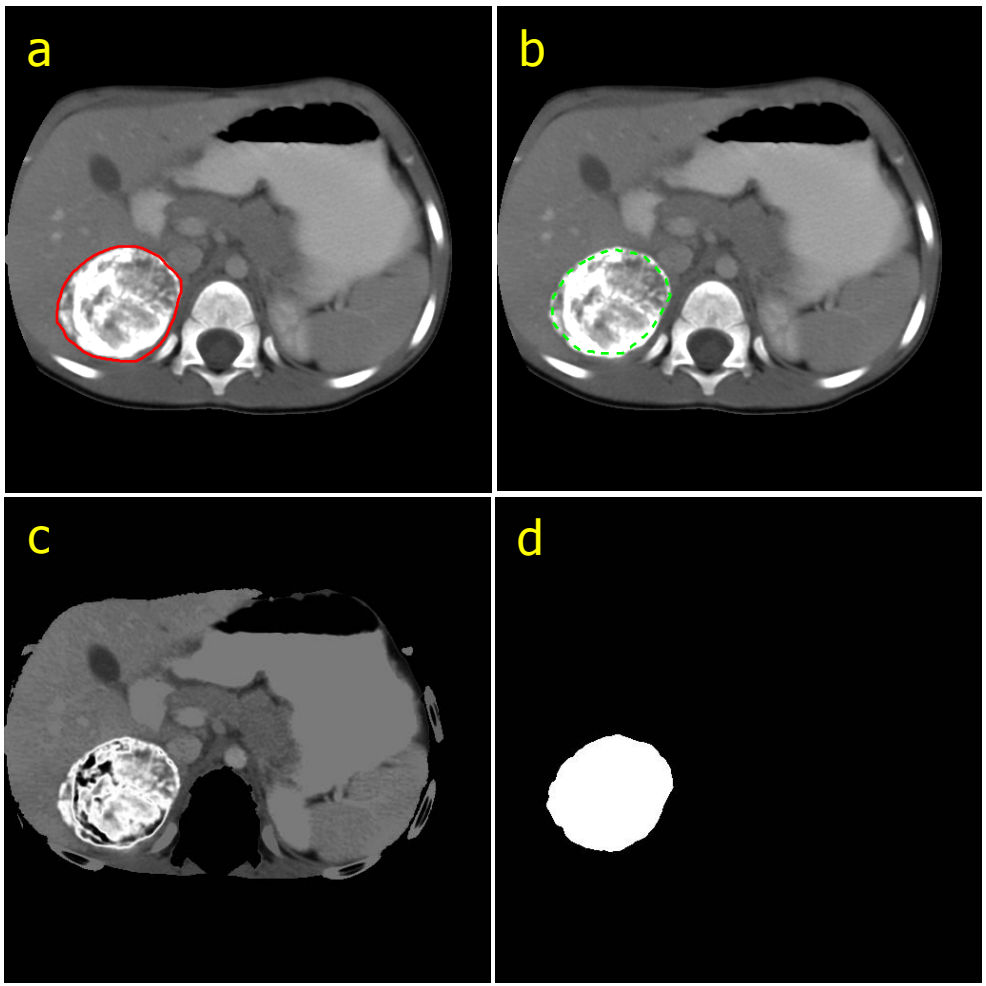

a. tumor segmented by a radiologist

b. user-selected region marker

c. result of opening-by-reconstruction

d. final result of segmentation

Segmentation of Neuroblastoma: Heterogeneous Tumor

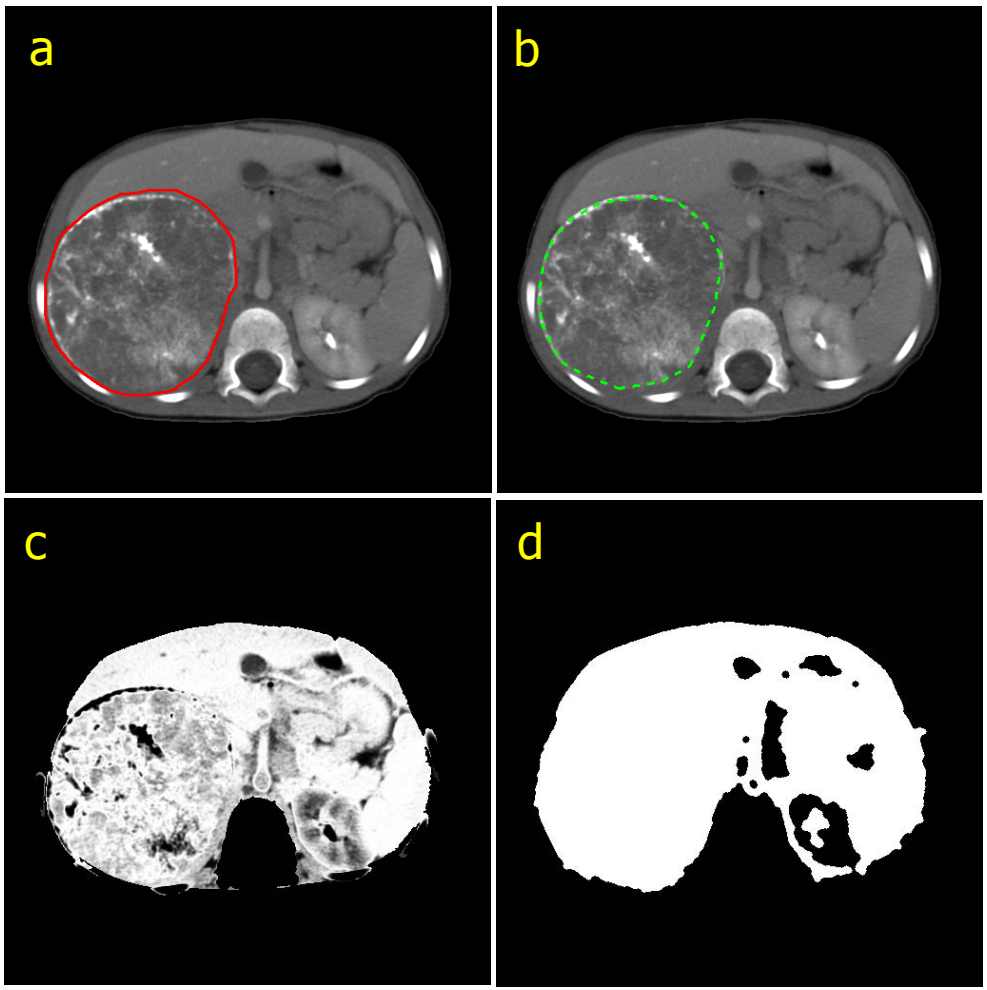

a. tumor segmented by a radiologist

b. user-selected region marker

c. result of opening-by-reconstruction

d. final result of segmentation

Segmentation of Neuroblastoma: Diffuse Tumor

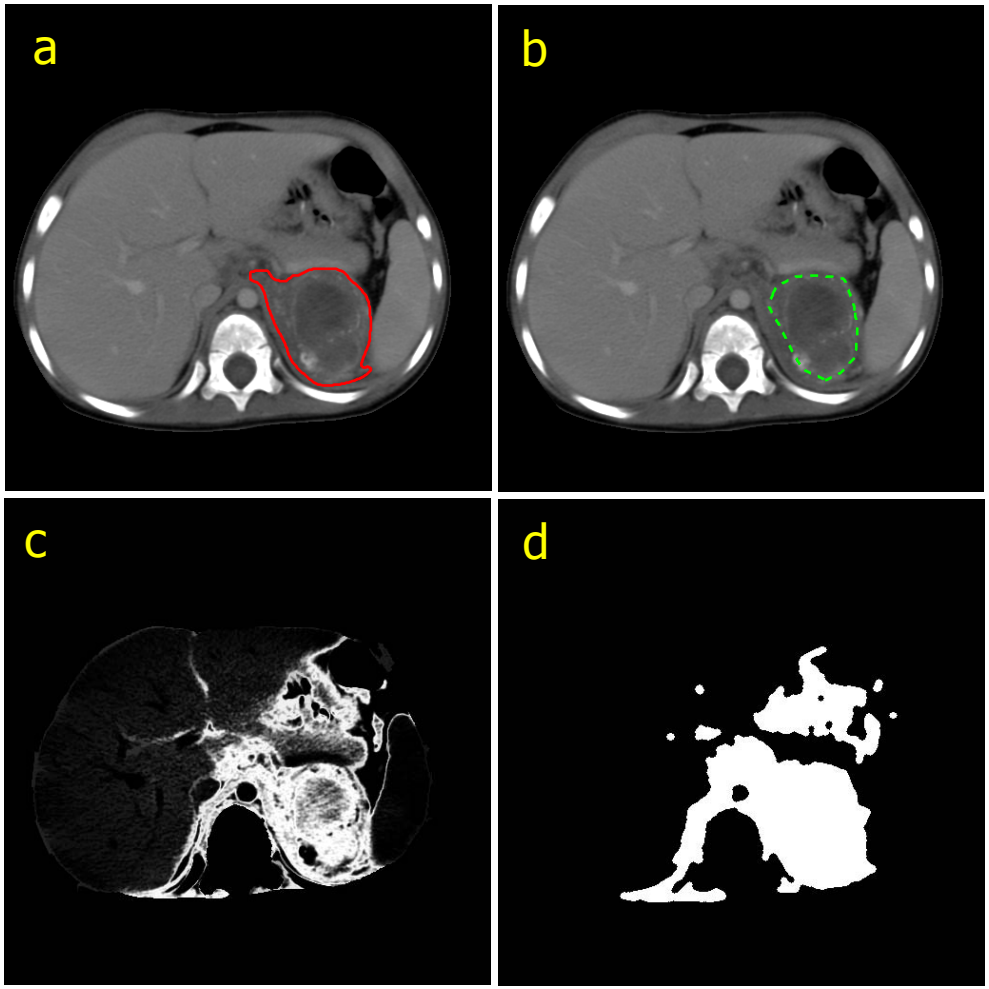

a. tumor segmented by a radiologist

b. user-selected region marker

c. result of opening-by-reconstruction

d. final result of segmentation

Result of Segmentation: Homogeneous Tumor

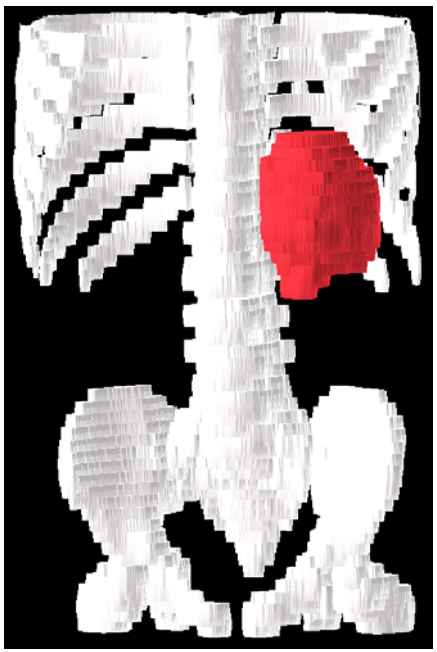

Tumor segmented by a radiologist

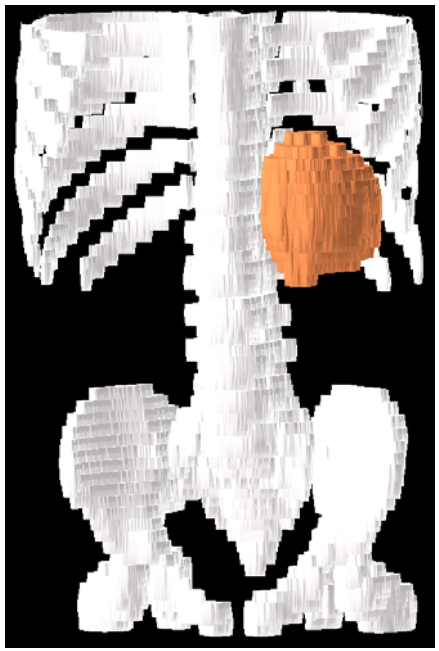

Initial result of tumor segmentation

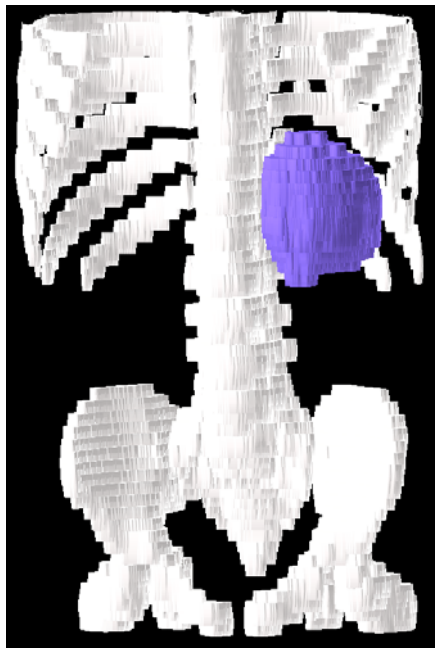

After removal of the thoracic cavity

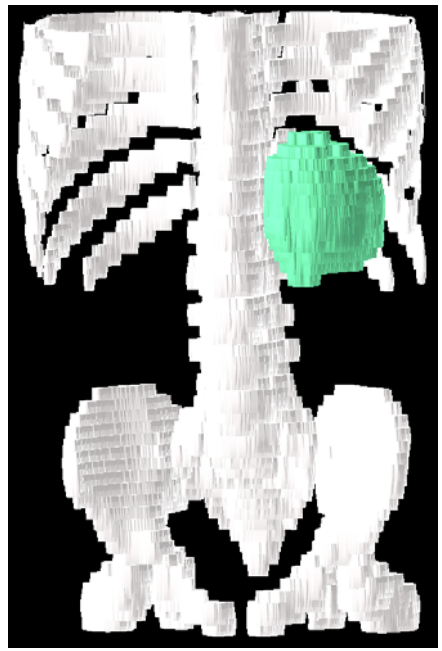

After removal of regions below the pelvic surface

Result of Segmentation: Heterogeneous Tumor

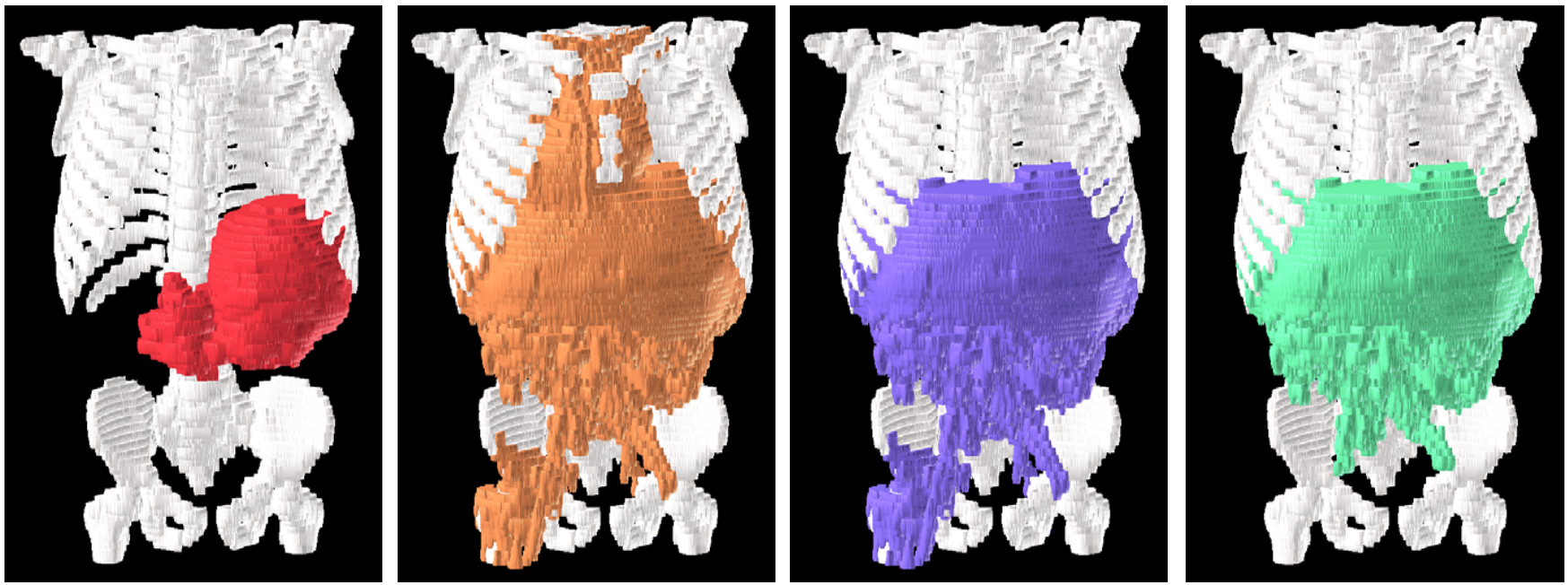

Tumor segmented by a radiologist

Initial result of tumor segmentation

After removal of the thoracic cavity

After removal of regions below the pelvic surface

Result of Segmentation: Diffuse Tumor

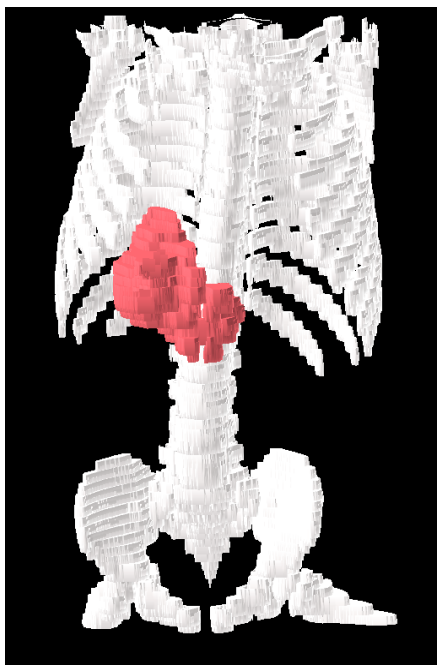

Tumor segmented by a radiologist

Initial result of tumor segmentation

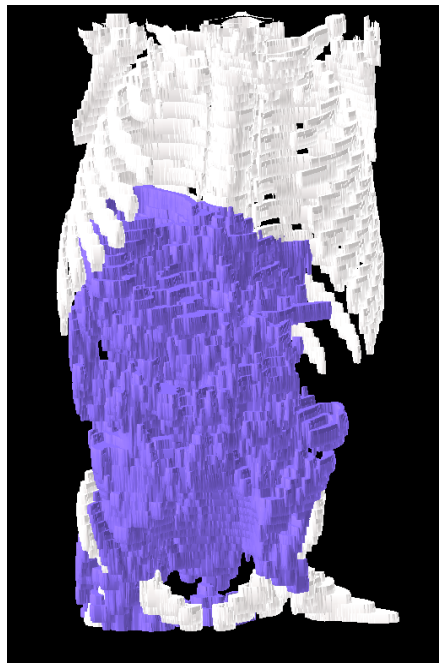

After removal of the thoracic cavity

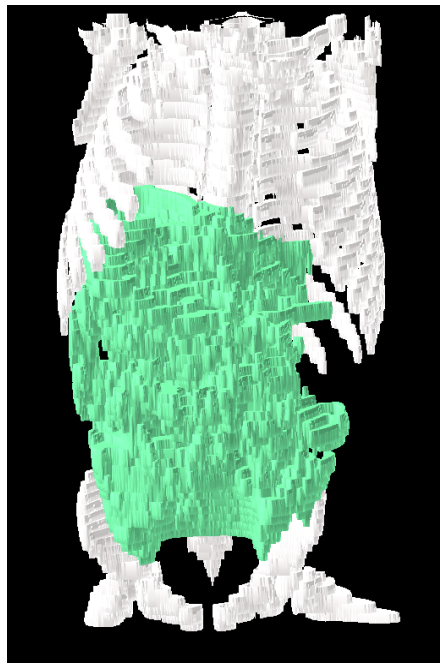

After removal of regions below the pelvic surface

Results

Exam	Initial result of segmentation (I)			Result of segmentation with prior removal of the diaphragm (II)					Result of segmentation with prior removal of the vertebral column and the region inferior to the upper pelvic surface (III)			
	ε_T	ε_{FP}	ε_{TP}	ε_T	ε_{FP}	ε_{TP}	% *Change* in ε_T	% *Change* in ε_{FP}	ε_T	ε_{FP}	% *Change* in ε_T	% *Change* in ε_{FP}
1A	244.9	265.7	79.2	200.6	221.4	79.2	-18.1	-16.7	180.7	201.7	-9.9	-8.9
1B	861.4	868.1	93.4	681.7	688.4	93.4	-20.9	-20.7	560.6	567.2	-17.8	-17.6
1C	-15.6	0.8	83.5	-15.6	0.8	83.5	0.0	0.0	-15.6	0.8	0.0	0.0
2A	115.3	127.7	87.5	95.3	109.4	85.9	-17.3	-14.3	59.6	73.7	-37.5	-32.6
2B	1376.9	1382.1	94.8	1118.7	1123.9	94.8	-18.8	-18.7	898.4	903.6	-19.7	-19.6
3A	1399.9	1416.9	83.0	1385.2	1402.2	83.0	-1.1	-1.0	1385.0	1402.0	0.0	0.0
3B	7552.0	7610.4	41.6	7066.2	7124.5	41.6	-6.4	-6.4	7066.2	7124.5	0.0	0.0
4A	-8.4	18.6	73.0	-9.2	18.0	73.0	9.5	-3.2	-10.4	17.0	13.0	-5.6
4B	683.4	690.1	93.3	674.1	680.9	93.3	-1.4	-1.3	551.6	558.3	-18.2	-18.0
4D	678.1	684.3	93.8	672.1	678.3	93.8	-0.9	-0.9	670.7	676.9	-0.2	-0.2
Average	1288.8	1306.5	82.3	1186.9	1204.8	82.1	-7.5	- 8.3	1134.7	1152.6	-9.0	-10.3

Results

- Effect of removal of the thoracic cavity: false-positive rate reduced by **8.3%**, on the average, over 10 CT exams of four patients.

- Effect of removal of the vertebral column and the regions below the pelvic surface: false-positive rate reduced by **10.3%**, on the average.

- True-positive rate: **82.1%**, on the average.

Conclusion

The proposed methods:

- separate the thoracic, abdominal, and pelvic cavities for further consideration;
- facilitate atlas-based and landmark-based approaches to segmentation of medical images;
- aid in reducing the false-positive error rate in the result of segmentation of tumors.

Future work

- Incorporation of other abdominal, thoracic, and pelvic landmarks.
- Extension of the methods to other imaging modalities.
- Implementation of competitive region growing for segmentation of multiple organs and tumors.
- Estimation of tissue composition in tumor mass using Gaussian mixture model.

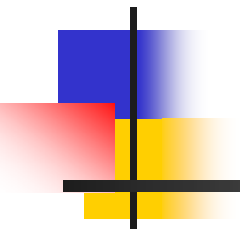

Thank you

This work is supported by a grant from the Natural Sciences and Engineering Research Council (NSERC) of Canada.

We thank Hanford Deglint and Randy Vu for their contributions to this project.